SIMULATION AND REALIZATION OF LLC CHARGER WITH PLANAR TRANSFORMER IN AVIATION APPLICATIONS

EREN ERDOĞAN

SEPTEMBER 2025

ÇANKAYA UNIVERSITY

GRADUATE SCHOOL

ELECTRICAL-ELECTRONICS ENGINEERING DEPARTMENT
ELECTRICAL-ELECTRONICS ENGINEERING MASTER'S THESIS

SIMULATION AND REALIZATION OF LLC CHARGER WITH PLANAR TRANSFORMER IN AVIATION APPLICATIONS

EREN ERDOĞAN

SEPTEMBER 2025

ABSTRACT

SIMULATION AND REALIZATION OF LLC CHARGER WITH PLANAR TRANSFORMER IN AVIATION APPLICATIONS

ERDOĞAN, EREN
ELECTRICAL-ELECTRONICS ENGINEERING MASTER'S THESIS

Supervisor: Prof. Dr. İres İSKENDER
September 2025, 97 pages

This thesis presents the end-to-end design, digital control, simulation, and experimental validation of a high-efficiency LLC resonant charger with a wide regulation range for aircraft batteries interfaced to a 270 VDC bus. Driven by stringent mass/volume constraints and reliability targets in aviation, soft-switching and step-up capability are required; the LLC topology is therefore adopted as it natively supports CC/CV (Constant Voltage/ Constant Current) charging.

The design proceeds from battery-imposed requirements and the 270 VDC input interface. The resonant tank is dimensioned by extracting m (Inductance ratio), Q (Quality factor), and R_ac (Equivalent AC resistance) from voltage-gain curves. After selecting fr (Resonant frequency), Lr (Resonant inductance), Cr (Resonant capacitance), and Lm (Magnetizing inductance) are computed and then refined with practical component choices. Selection criteria for a high-frequency planar transformer are defined, suitable Si/SiC switching devices are assessed, and the output rectification architecture is chosen to maximize efficiency and to interface cleanly with digital control.

Control uses frequency modulation with a PI regulator to realize closed-loop current and voltage regulation via a pulse-frequency modulator. Operation at, above, and below resontracksis analyzed in simulation; the results show that the topology and

the implemented digital closed loop track the CC/CV profile appropriately for battery charging.

Experimental work on a laboratory prototype confirms soft-switching conditions, the gain–frequency behavior, and CC/CV regulation. The measurements meet the targeted efficiency and operating range, and they align with the simulated trends.

Chapter 1 explains the project aim and literature survey, Chapter 2 motivation for aviation electrification, battery history, the role of charging systems, and the rationale for resonant conversion. Chapter 3 states, the 270 VDC and battery-driven requirements, and the basis for topology selection. Chapter 4 presents the high-level architecture and block diagrams for power and control/data flow. Chapter 5 details the LLC structure, resonant-tank equations and workflow, computation of Lr, Cr, Lm, and the transformer, semiconductor, and rectification choices. Chapter 6 describes the digital controller platform, frequency-modulation strategy, and PI-based closed-loop design. Chapter 7 reports the simulation setup, gain-curve extraction, and CC/CV performance analyses. Chapter 8 provides prototype test results.

Keywords: LLC resonant converter, Aircraft batteries, Soft switching, Frequency-modulated digital control, Planar transformer, Aviation battery charger.

ÖZET

HAVACILIK UYGULAMALARINDA DÜZLEMSEL TRANSFORMATÖRLÜ LLC ŞARJ CİHAZININ SIMÜLASYONU VE GERÇEKLEŞTİRİLMESİ

ERDOĞAN, EREN
ELEKTRİK-ELEKTRONİK MÜHENDİSLİĞİ YÜKSEK LİSANS TEZİ

Danışman: Prof. Dr. İres İSKENDER
Eylül 2025, 97 Sayfa

Bu tez, 270 VDC baraya bağlı uçak bataryaları için yüksek verimli ve geniş regülasyon aralığına sahip bir LLC rezonanslı şarj cihazının uçtan uca tasarımını, sayısal denetimini, simülasyonunu ve deneysel doğrulamasını sunar. Havacılıkta kütle/hacim kısıtları ve güvenilirlik hedefleri nedeniyle yumuşak anahtarlama ve yükseltici çalışma yeteneği olan topolojiler gereklidir; bu bağlamda CC/CV (Sabit Akım / Sabit Gerilim) profilini doğal olarak destekleyen LLC topolojisi seçilmiştir.

Tasarım, batarya dayatmaları ve 270 VDC giriş arayüzüyle tanımlanan gereksinimlerden başlayarak rezonant tankın kazanç eğrileri üzerinden m (Endüktans oranı), Q (Kalite faktörü) ve Rac (Eşdeğer AC direnci) parametrelerinin çıkarımıyla boyutlandırılmasını içerir. fr seçimi sonrası Lr (Rezonans endüktansı), Cr (Rezonans kapasitansı), Lm (Manyetik endüktansı) değerleri hesaplanmış, pratik bileşen seçimleriyle güncellenmiştir. Yüksek frekanslı planar transformatör için seçim kriterleri belirtilmiş, anahtarlama elemanları olarak uygun Si/SiC cihazları değerlendirilmiştir. Çıkış doğrultma mimarisi hem verimi artıracak hem de dijital kontrol ile rahatlıkla yönetilebilecek şekilde seçilmiştir.

Denetimde frekans modülasyonu temelli bir mimari ve PI kontrolcü kullanılmış; darbeli frekans modülatörü ile kapalı çevrim akım/gerilim regülasyonu gerçekleştirilmiştir. Kurulan modelle rezonans, üstü ve altı çalışma bölgeleri analiz

edilmiş; simülasyon sonunda, topolojinin ve kurulan dijital kapalı çevrim kontrolün batarya sarjına uyumlu davrandığı görülmüştür.

Deneysel çalışma, laboratuvar prototipi üzerinde yumuşak anahtarlama koşullarını, kazanç–frekans davranışını ve CC/CV regülasyonunu doğrular. Seçilen mimarinin verim ve çalışma aralığı hedeflerini karşıladığı görülür.

Bölüm 1: Proje amacı ve literatür tarama, Bölüm 2: Havacılıkta elektrifikasyon motivasyonu, batarya tarihi, şarj sistemlerinin önemi ve rezonanslı çevirici tercihinin gerekçesi açıklar Bölüm 3: 270 VDC giriş ve batarya kaynaklı gereksinimler, topoloji seçiminin dayanaklarını belirtir. Bölüm 4: Güç ve kontrol/veri akışı için yüksek seviyeli mimari ve blok diyagramları göstermektedir. Bölüm 5: LLC yapısı, rezonant tank denklemleri ve akışı; Lr, Cr, Lm hesaplanması, planar transformatör ve yarıiletken/doğrultma seçimi gibi konuları ayrıntılı şekilde açıklar. Bölüm 6: Sayısal denetleyici platformu, frekans modülasyonu ve PI tabanlı kapalı çevrim tasarımını anlatır. Bölüm 7: Simülasyon kurulumu, kazanç eğrisi çıkarımı ve CC/CV performans analizlerini gösterir. Bölüm 8: Prototip üzerinde gerçekleştirilen testlerin sonuçlarını içerir.

Anahtar Kelimeler: LLC rezonanslı dönüştürücü, Hava aracı bataryaları, Yumuşak anahtarlama, Frekans modülasyonlu sayısal kontrol, Planar transformatör, Havacılık Sarj Cihazı.

ACKNOWLEDGEMENT

An advisor I would very much like to thank Prof. Dr. İres İSKENDER for providing scientific guidance, giving constructive criticism, and leading the way during my thesis work.

I am thankful to Aspilsan Enerji and all my coworkers for their support in terms of infrastructure, providing laboratory facilities, and giving technical assistance for the product realization that was designed within the scope of this work. Especially to Ali Kaan ÜNSAL for his contributions to the design, verification, and testing phases. The technical discussions and feedback during the planning, documentation, and publication-preparation stages were instrumental in the refinement of this thesis.

I thank my family: my mother, Nuran ERDOĞAN, my father, Hüseyin ERDOĞAN, and my sister İrem ERDOĞAN for their unwavering support throughout my education.

I also owe special thanks to my spouse, Kübra ÇİLOĞLU ERDOĞAN, for her financial and moral support, patience, and dedication throughout my academic journey. This work could not have been completed without the contributions of the individuals and institutions mentioned above.

TABLE OF CONTENTS

LIST OF TABLES

LIST OF FIGURES

LIST OF SYMBOLS AND ABBREVIATIONS

SYMBOLS

V	: Volt
A	: Amper
W	: Watt
H	: Henry
F	: Farad
g	: Gram
Ω	: Ohm
C	: Coulomb

ABBREVIATIONS

AC	: Alternating Current
ADC	: Analog-to-Digital Converter
Ae	: Effective Core Area
APU	: Auxiliary Power Unit
Bmax	: Maximum Flux Density
BMS	: Battery Management System
CC	: Constant Current
Cr	: Resonant Capacitor
CV	: Constant Voltage
DC	: Direct Current
EMI	: Electromagnetic Interference
EPWM	: Enhanced Pulse-Width Modulation
eVTOL	: electric Vertical Take-Off and Landing
FET	: Field-Effect Transistor
FPGA	: Field-Programmable Gate Array
FPU	: Floating-Point Unit
fr	: Resonant Frequency

Fx	: Fundamental Frequency
H²PAK	: Power MOSFET Package
Id	: Drain Current
ILr	: Resonant Inductor Current
IREF	: Reference Current
K	: Gain
k	: Steinmetz Coefficient
Ki	: Integral Gain
Kp	: Proportional Gain
Li-ion	: Lithium-ion
LLC	: Inductor–Inductor–Capacitor Resonant Converter
Lm	: Magnetizing Inductance
Lr	: Resonant Inductance
LRU	: Line-Replaceable Unit
m	: Lm/Lr Ratio
MCU	: Microcontroller Unit
MIPS	: Million Instructions Per Second
n	: Turns Ratio (Np/Ns)
Ni-Cd	: Nickel–Cadmium
Np	: Primary Turns
Ns	: Secondary Turns
PCB	: Printed Circuit Board
PFM	: Pulse-Frequency Modulation
PI	: Proportional–Integral Controller
Po	: Output Power
PWM	: Pulse-Width Modulation
Q	: Quality Factor
Qgs	: Gate-to-Source Charge
Rac	: Equivalent AC Load Resistance
Rdson	: Drain–Source On-Resistance
RMS	: Root Mean Square
Ro	: Output/Load Resistance
SMD	: Surface-Mount Device

SR	: Synchronous Rectification
Ts	: Switching Period
TVS	: Transient Voltage Suppressor
UAV	: Unmanned Aerial Vehicle
VDC	: DC Voltage
VDS	: Drain–Source Voltage
Ve	: Effective Core Volume
Vf	: Forward Voltage
Vin	: Input Voltage
Vo	: Output Voltage
Vout	: Output Voltage
VREF	: Reference Voltage
ZCS	: Zero-Current Switching
ZVS	: Zero-Voltage Switching
α	: Steinmetz Frequency Exponent
β	: Steinmetz Flux-Density Exponent

CHAPTER I
INTRODUCTION

1.1 THESIS OVERVIEW AND PURPOSE

The purpose of this study is to design a high-efficiency charger for charging high-voltage batteries used in aircraft, to prototype this design, and demonstrate its performance. It also aims to demonstrate the feasibility of this topology for converters used in aircraft.

1.2 LITERATURE SURVEY

1.2.1 The More-Electric Aircraft and Beyond

In the study titled The More-Electric Aircraft and Beyond, the historical development and the future role of aircraft electrification are comprehensively discussed. The authors emphasize that, in response to increasing air traffic, improving aircraft performance requires the combined consideration of power electronics, electrical machine design, control systems, thermal management, manufacturing engineering, and new material technologies. In particular, they state that achieving goals such as power density, reliability of the system and availability cannot be achieved by individually optimizing the components, but requires a system approach for the design. The study points out further that with regard to the selection of the topologies of the power electronics, the thermal design, the methods of design and manufacture and the means of integration must be regarded from early stages of the design. From this it is shown that in the electrical power distribution systems of the aircraft, the topology selection is dictated not only by electrical factors, but also by mechanical and thermal constraints. At present, the MEA (More Electric Aircraft) concept has already entered commercial service with consolidated products, while FEA (Fully Electric Aircraft) products have reached the stages of certification and commercialization [1].

In conclusion, aircraft electrification is no longer limited to the electrification of specific subsystems but signals a transformation toward fully electric aircraft becoming an integral part of everyday life. In this context, the systems approach presented in the study supports the view that LLC-based power converters, offering high efficiency and reliability, can also become fundamental building blocks of aircraft electrification. In particular, LLC solutions that provide high power density and a reliable charging infrastructure will play a critical role on the path toward the MEA and FEA vision.

1.2.2 High-Efficiency Hybrid LLC Resonant Converter for On-Board Chargers of Plug-In Electric Vehicles

In the paper titled High-Efficiency Hybrid LLC Resonant Converter for On-Board Chargers of Plug-In Electric Vehicles, a hybrid LLC converter capable of operating in three distinct modes is proposed for CC–CV charging of electric vehicle batteries. Experimental results show that, compared with the conventional full-bridge LLC topology, the proposed hybrid structure achieves an efficiency improvement of approximately 1% at low voltage and 2.3% under light load conditions. The designed 3.2 kW GaN-based prototype reaches a power density of 65 W/in³ and delivers a peak efficiency of 98.5%, while maintaining nearly constant efficiency across the entire load range. In addition, the control strategy enables smooth transitions between CC and CV modes, thereby improving regulation performance. Although this work is directly focused on EV chargers, the demonstrated features of high efficiency, compact design, and high power density are of critical importance for aviation applications. Under the strict volume and weight constraints of aircraft, such hybrid LLC topologies make it possible to design high-power battery chargers that are both reliable and efficient [2].

1.2.3 Burst Mode Elimination in High-Power LLC Resonant Battery Charger for Electric Vehicles

In the paper titled Burst Mode Elimination in High-Power LLC Resonant Battery Charger for Electric Vehicles, a specially designed LLC resonant converter and control strategy are presented for high-power battery charging applications. The LLC tank circuit, including leakage inductance, is modeled at higher order, and normalized parameters are mathematically optimized. As a result, the converter

achieves soft switching (ZVS/ZCS) of semiconductor devices under all operating conditions and regulates the output voltage from nearly 0 V up to 1.5 times nominal with only minor changes in switching frequency [3].

Experimental results confirm that the proposed strategy allows the converter to cover almost the entire V–I plane and operate with a peak efficiency of 96.5%. Though this study intends to be focused on EV chargers only, the disclosed characteristics of a stable current profile, high efficiency and a wide voltage regulation clearly point to the adaptability of LLC topology in aviation applications where a reliable current quality and a high degree of performance are very important [3].

1.2.4 A Novel Re-configurable LLC Converter for Electric Aircraft

The paper titled A Novel Re-configurable LLC Converter for Electric Aircraft reviews a reconfigurable LLC topology that can tolerate any faulty state of the power converter, that has been made suitable for applications in aircraft. The design contains six additional semiconductor switches and a specially wounded transformer, which allows the converter to be able to go from one operating mode to another, if a fault condition is encountered. For instance, if a switch in the primary full-bridge fails, the converter automatically switches to half-bridge LLC mode and the output is maintained in service. In the case of an open-circuit fault condition developing in the secondary rectifier diodes of the converter, the circuitry is also reconfigured so that power is still delivered without interruption [4].

Because of this adaptability, the converter can ride through a single-point failure without immediately sacrificing overall reliability in flight. From the angle of mission continuity, which tends to matter more than anything else in aviation, reconfigurable LLC converters become a pretty practical way to satisfy strict reliability targets. They do not magically remove failure modes, of course, but they help the system absorb them in a controlled, predictable way [4].

1.2.5 Topology-Reconfigurable Fault-Tolerant LLC Converter with High Reliability and Low Cost for More Electric Aircraft

In the paper Topology-Reconfigurable Fault-Tolerant LLC Converter With High Reliability and Low Cost for More Electric Aircraft, a cost-effective approach is introduced to provide a reliability close to more complex reconfigurable solutions. With the addition of only two extra diodes in the presented design, operation continuity

can be achieved even after two consecutive switch failures. Hence, this enables high fault tolerance with minimal extra hardware [5].

Importantly, the dynamic behavior of the converter is mostly preserved both before and after faults, and there is no need for complex redesign of the control system. Prototype experiments verify that the output will still remain stable in case of faults and prove the practicality of the method proposed in [5].

This work deals with the importance of weight and cost in aerospace systems and, therefore, indicates that LLC-based solutions can provide high reliability at very low additional cost, enhancing their applicability in the electrification of aircraft [5].

1.2.6 Snubberless Bidirectional DC–DC Converter With New CLLC Resonant Tank Featuring Minimized Switching Loss

I In the paper presented, Snubberless Bidirectional DC–DC Converter With New CLLC Resonant Tank Featuring Minimized Switching Loss, Chen et al. (2010) propose a novel CLLC resonant DC–DC converter topology with high efficiency and minimizing switching loss that is capable of bidirectional power transfer. An L–C–L–C resonant tank is coupled symmetrically on both the primary and secondary sides to facilitate soft switching conditions for power flow in either direction. In particular, the primary switches realize ZVS, and the secondary rectifier or synchronous devices achieve ZCS, hence no external snubber circuit is required to eliminate the switching losses altogether [6].

The authors prove the concept with a 500 VA prototype able to operate bidirectionally between 400 V and 48 V. Experimental results show that the converter offers efficiencies higher than 96% in both buck (step-down) and boost (step-up) modes, confirming the CLLC topology intrinsic advantages in reducing switching losses and electromagnetic interference [6].

Although the study is mainly oriented toward applications such as electric ground vehicles, uninterruptible power supplies, and renewable energy systems, its findings are highly relevant to aviation. Of particular value to aerospace battery systems, where both charging and regenerative power feedback may be required, is the ability of soft-switched bidirectional LLC-derived topologies to provide high efficiency and high reliability simultaneously. Such converters could improve flight safety and energy management performance and thus are strong candidates for future aircraft electrification architectures [6].

1.2.7 Loss Analysis of Full Bridge LLC Resonant Converter with Wide Input Range Using Si and SiC Switches

In the paper Loss Analysis of Full Bridge LLC Resonant Converter with Wide Input Range Using Si and SiC Switches, Farooq et al. (2021) compare the performance of Si MOSFETs and SiC MOSFETs in a 3 kW full-bridge LLC resonant converter operating over a wide input voltage range. Simulation results analyze separately the conduction and switching losses under various voltage and load conditions and provide several important conclusions. Among them is that for higher input voltages, there is a serious efficiency drop-off for Si MOSFETs. For example, at 400 V of input voltage, the Si-based design delivers only about 93% efficiency. In contrast, the SiC-based design attains much higher efficiency and continues to have reduced switching losses under light load [7].

In this study, it is further demonstrated that SiC devices allow higher frequency and elevated operating temperature, hence higher power density in LLC converters. The authors, though, also point out the question of cost for SiC technology and the balance between cost and performance in view of the target application [7].

While this research has primarily focused on terrestrial applications, its results relate directly to aerospace as well. Efficient and lightweight features are of utmost priority in aeronautical power electronic technologies; therefore, SiC-based LLC solutions can minimize losses in aircraft high-voltage DC bus architectures, helping to develop more compact, lightweight, and reliable chargers, provided that issues with cost and certification are resolved [7].

CHAPTER II
AVIATION ELECTRIFICATION

2.1 MOTIVATION FOR ELECTRIFICATION IN AVIATION

The aviation sector is quickly embracing electric and hybrid technologies [8]. Innovations like electric vertical take-off and landing (eVTOL) aircraft, unmanned aerial vehicles (UAVs), and auxiliary power units (APUs) in traditional aircraft are driving a growing need for batteries with high energy density and more efficient power conversion systems [1], [8]. In an aircraft's electrical system, batteries fulfill three critical roles. First, they supply the initial power for system startup. Second, they maintain stability on the DC bus by absorbing transient loads. Most critically, they function as a short-term, high-integrity power source to ensure safety during emergencies [9].

As aviation moves toward electrification, the design of battery and charging systems becomes critical. This criticality is underscored by the fact that modern aircraft rely on sophisticated battery chargers to maintain the battery at a high state of charge during normal flight operations, thereby ensuring its readiness should it be required as the sole power source [9]. The low efficiency of traditional power supplies—such as linear regulators and PWM-based hard-switched systems—presents a major obstacle. This inefficiency directly results in heavier and bulkier power systems, imposing a severe penalty where every gram counts: the aircraft's design [10]. This is exactly why resonant converters are becoming the most popular technology for modern aircraft. They have a clear path to the lighter, smaller systems that modern aviation needs because they are very efficient and have a lot of power.

LLC resonant converters satisfy these needs by providing the lightweight, compact, and efficient charging solutions that are essential for aerospace applications. So, this thesis gives a full performance analysis of a certain LLC resonant converter that uses a planar transformer and was made just for charging aircraft batteries.

2.2 GENERAL HISTORY OF AIRCRAFT BATTERIES

Lead-acid batteries were the first to be used in the aviation sector in the early 1900s. Batteries were mainly used to power emergency systems and aid engines starting in early-generation aircraft. However, the switch to nickel-cadmium (Ni-Cd) and lithium-ion (Li-ion) batteries was ultimately necessitated by the low energy density, substantial weight, and sizable size of lead-acid batteries [11,12].

An overview of the evolutionary development of battery technologies in the aviation sector can be summarized as follows:

1970s – 1990s: Ni-Cd batteries were widely used in commercial aircraft. Nevertheless, drawbacks such as memory effect, low energy density, and the presence of toxic substances limited their range of applications [11,12].

From 2000 onwards, Li-ion batteries have quickly gained adoption in aviation thanks to their lightweight and high energy density. Modern passenger aircraft such as the Boeing 787 Dreamliner and the Airbus A350 now use Li-ion batteries extensively [13].

The main reasons for the widespread use of Li-ion batteries in the aviation sector include:

- Higher energy density: Facilitates extended duration of flight operations, consequently enhancing overall operational efficiency.
- Reduced weight: Facilitates enhancements in fuel efficiency while enabling aircraft to transport increased cargo capacities.
- Longer cycle life: Lowers battery replacement and maintenance expenses, offering economic benefits.
- Greater charge-discharge efficiency: Minimizes energy losses and enhances overall system performance.

However, because Li-ion batteries carry risks such as thermal runaway and overheating, advanced battery management systems (BMS) and safe charging solutions are essential. Consequently, aviation applications incorporate smart battery monitoring, temperature management, and stringent safety protocols into their charging technologies [14].

2.3 IMPORTANCE OF CHARGING SYSTEMS IN AIRCRAFT

In modern aircraft, the battery is much more than an auxiliary device; it forms part of the robust heart of the electrical system that supports the main engines and a host of flight-critical components. It also supports advanced flight controls serving as the aircraft's digital nervous system, hydraulic and pneumatic support units acting like its muscles, and much more. In addition to this, batteries also contribute to efficiencies in new operational facets, such as electric taxi systems. Most fundamentally, batteries provide an ultimate fail-safe, delivering high integrity power to all emergency systems when everything else has failed [9].

Since these systems have to work continuously and uninterruptedly in service, increasing demands are put on the efficiency, safety, and light weight of charging systems. Classic switched-mode power supplies have problems related to switching losses and EMI at high operating frequencies. Therefore, LLC resonant converters which can solve these problems are a good solution for power conversion in aircraft applications. [15].

LLC resonant converters are widely employed in aircraft battery charging systems due to the following reasons:

High efficiency: They reduce the switching losses by zero-voltage and zero-current switching techniques [5,16,17,18].

EMI Compatibility: They produce less electromagnetic noise, enhancing their compatibility with avionics systems [15].

Lightweight, compact design: Smaller transformers and components reduce total weight in aircraft design systems [19].

Among other methods, LLC resonant converters are considered the most promising technology in aircraft battery charging systems due to their capability for assured reliability and weight optimization.

2.4 IMPORTANCE OF WEIGHT AND SIZE IN AIRCRAFT APPLICATIONS

In aerospace, there's simply no getting away from the obsession with cutting weight. It is one of those things that keeps cropping up: shave off a bit here, save some fuel there, and suddenly you're looking at a big difference over time. It does not matter if the weight savings seem minuscule upfront; aircraft manufacturers know that every single pound can make a noticeable impact, both on fuel bills and how the plane

actually handles in the air. So, the search for anything that can be made lighter is pretty much constant in this field. Curiously enough, studies have revealed that shaving off just a small amount from a single component might actually result in notable fuel savings over the years an aircraft is in service. Because of this, systems supplying power have always been under a lot of pressure. Traditional transformers are a good example of such systems - the old wire-wound type. They work, but their size and heaviness have long made it tough to ramp up the power density without adding unwanted bulk.

Planar transformers have really shaken things up in this area. Instead of winding wires around a core like in the old days, these newer models use traces built right into printed circuit boards. That alone makes them much flatter and lets engineers fit them into tighter spaces-something that's always in short supply in airplanes. There's more to it, though: planar designs tend to handle heat better and lose less energy to magnetics, which means they're not just lighter but also a bit more efficient at their job. By being able to squeeze more power through a smaller device, planar transformers hit exactly what today's aviation electronics need most.

It is when you combine planar transformers with an LLC resonant converter that they really come into their own. In this hybrid, the high-frequency, low-loss switching features of the LLC topology combine with the streamlined, thermally efficient build of planar magnetics. This technological combination is particularly advantageous in airplane battery charging applications because these require compactness, light weight, and optimum efficiency. Eventually, the integration of these systems offers a robust answer to the evolving demands of next-generation aviation electronics.

2.5 ADVANTAGE OF RESONANT CONVERTERS

Resonant converters offer higher efficiencies and less switching losses than traditional PWM-based converters [20]. Because of these benefits, they are the first choice by far in the power-density-critical applications, for example, in the field of aviation.

The advantage of resonant converters include:

Minimizing switching losses using soft switching techniques [21].

Operating at higher frequencies, allowing transformer size reduction and weight optimization.

Reduced electromagnetic interference (EMI) levels, ensuring better compatibility with aviation systems [21].

2.6 STRUCTURE OF THE THESIS

Chapter 1: Thesis overview, purpuse and literature survey.

Chapter 2: Motivation for aviation electrification, battery history, role of charging systems, rationale for resonant conversion.

Chapter 3: 270 VDC and battery-driven requirements, basis for topology selection.

Chapter 4: High-level architecture and block diagrams for power and control/data flow.

Chapter 5: LLC structure, resonant-tank equations and workflow, computation of Lr, Cr, Lm, and transformer/semiconductor/rectification choices.

Chapter 6: Digital controller platform, frequency-modulation strategy, PI-based closed-loop design.

Chapter 7: Simulation setup, gain-curve extraction, CC/CV performance analyses.

Chapter 8: Prototype test results.

CHAPTER III
DESIGN REQUIREMENTS AND SYSTEM OVERVIEW

3.1 DESIGN REQUIREMENTS AND TARGET SPECIFICATIONS

3.1.1 Input Interface to the 270 VDC Busbar

Modern, more electric aircraft use a 270 VDC busbar to minimize conductor weight while keeping insulation requirements manageable. This 270 VDC busbar will be the charger's input. While the input voltage can vary, it is assumed to be nominally 275 VDC, as the fully charged voltage of the backup battery will be 275 VDC. Generating a bus voltage below this voltage will deplete the battery's capacity.

3.1.2 Output Characteristics Imposed by the Battery Pack

The output performance and control algorithm of the designed charging device are entirely shaped by the electrical and chemical requirements of the target battery pack. The battery pack targeted in this work consists of 80 series-connected Lithium-ion (Li-ion) cells. To ensure this pack is charged in a safe, healthy, and efficient manner, the precise implementation of the industry-standard Constant Current - Constant Voltage (CC-CV) charging protocol, which is comprised of two consecutive phases, is required [22].

This protocol is a two-stage process designed to rapidly transfer energy into the battery at the commencement of the charge cycle via the CC phase, while safely completing the charge in the final stages without stressing the cells as the battery fully approaches capacity through the CV phase [22]. The control system of the charger is designed to execute a smooth and automatic transition between these two modes. The figure below shows the idealized profile of the entire charge cycle.

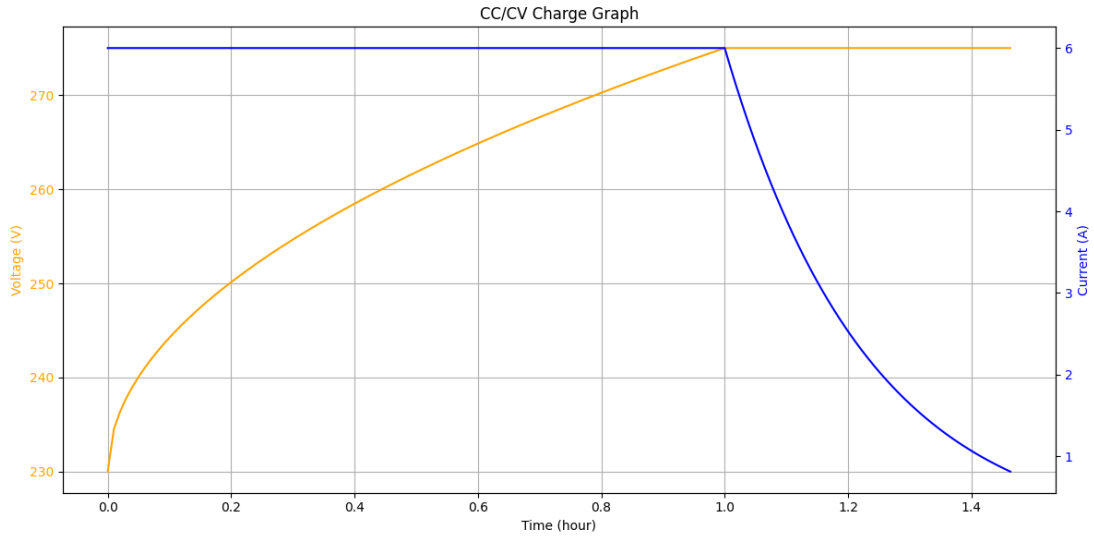

Figure 1: Represented CC/CV Charge Graph

3.1.2.1 Constant Current Charging Phase

This stage is the time when most of the energy is sent to the battery over the whole charging battery. In this stage, the main role of the controller is to limit the output current to a constant value if the battery voltage is lower than the full charge voltage.

- Nominal Charge Current: 6 A. It is this current that the controller should keep at a steady level all the time, even when the voltage of the battery is going up.

3.1.2.2 Constant Voltage Charging Phase

As the battery voltage rises with the charging process and gets to the full charge voltage of the pack of 275 V, the control system is switching automatically to CV mode. This step is to ensure that the cells are getting fully saturated and the charging is done in a safe way.

- Regulation Voltage: The output voltage should be kept at 275 V. In this moment when the voltage is kept constant, the current will gradually be decreasing, and the charger's output load will also be decreasing continuously. This is proof that the charger needs to be able to function stably even at low loads.

3.2 FINAL DESIGN SPECIFICATIONS

Table 1: Final Design Specifications

Parameter	Requirement
Input Voltage	240 - 275VDC
Output Voltage Range	230 – 280VDC
Output Current	6A
Maximum Output Power	1650W
Maximum Target Efficiency	%97

3.3 TOPOLOGY SELECTION AND JUSTIFICATION

3.3.1 Determining Topology Appropriate to Design Requirements

The choice of topology that determines the basic architecture of the power electronics system, has a very strong influence on the project parameters of the first order, such as efficiency, volume, cost, and performance. Hence, the system requirements were defined, and the preparatory work for the selection of the topology most suitable for these requirements was done prior to the topology selection. The key design objectives for this battery charger project are as follows:

1. Maximum Efficiency: To reduce thermal stress and maximize energy efficiency, particularly by minimizing switching losses.
2. Wide Regulation Range and Step-up Capability: To provide stable and efficient regulation across the wide output voltage range required by the battery charge cycle and to charge the battery to 100% even at low input voltages.

As a result of engineering evaluations conducted in line with these objectives, the LLC Resonant Converter topology was selected as the basis for the project. The following subsections present the fundamental technical rationale behind this choice, concerning the project's main objectives.

3.3.2 High Efficiency Target and Soft Switching

High efficiency is one of the primary goals of the project. In aviation applications, the weight and size of equipment are key factors influencing the choice. When you design a high-efficiency circuit, your thermal losses are reduced. This allows you to prepare the product for installation with a lighter heat sink.

The biggest obstacle to efficiency in high-power applications is the switching losses that occur when semiconductor switches are turned on and off. The problem in traditional "hard switching" topologies is that the switch is exposed simultaneously to high current and high voltage; this creates tremendous power loss and heat generation.

The LLC topology minimizes this by softly switching the switching elements due to the natural behavior of the resonant tank.

- Primary Side Zero Voltage Switching (ZVS): LLC produces a current flow in the resonant tank, which decreases the voltage across the switches to zero before the turn-on of the switches. Therefore, the switch can be turned on at zero voltage, and hence theoretically, turn-on switching losses are eliminated. This results in much better efficiency, particularly at high input voltages [6], [7].
- Zero Current Switching (ZCS) on the Secondary Side: Since the resonant current is sinusoidal in nature, the current through the output rectifier diodes automatically reaches zero. Since the diode turns off at zero current, the losses due to reverse recovery, which is a major loss factor in the hard-switched topologies, are eliminated [6], [7].

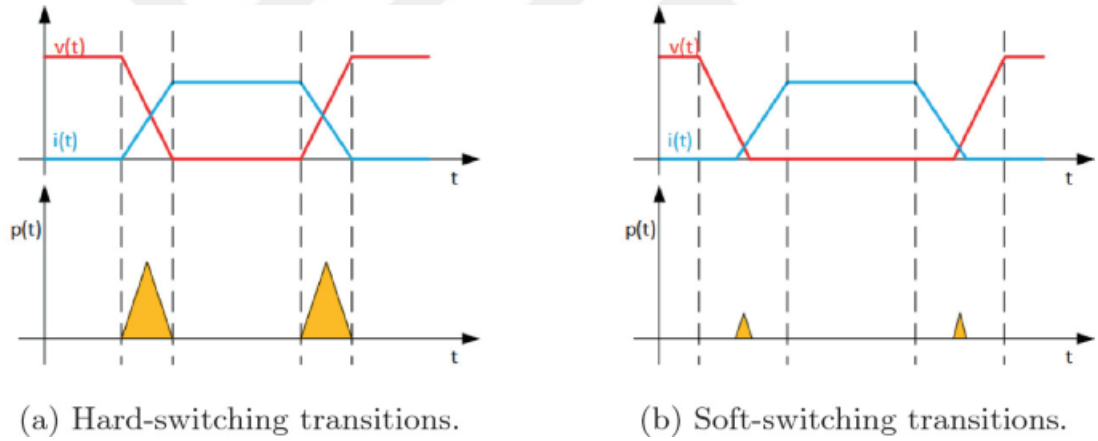

(a) Hard-switching transitions. (b) Soft-switching transitions.

Figure 2: Hard-Switching vs Soft-Switching

Therefore, the LLC topology is a structure that is by nature highly efficient due to its soft switching capability on both the primary and secondary sides, thus it is a direct way of achieving the project's primary goal.

3.3.3 Wide Regulation Range and Step-up Feature

The battery pack's operating voltage range that is to be charged makes it necessary for the selected topology to have a wide range of regulation capabilities. The LLC topology meets this requirement inherently because of its frequency-dependent gain characteristic, which is controlled by Pulse Frequency Modulation (PFM)[16].

By having a flexible gain structure, the charger becomes capable of delivering in an efficient way all voltage levels that are necessary depending on the battery's state of charge.

Furthermore, the inherently step-up (boost) feature that is available in the LLC topology when it is working below the resonant frequency (K>1) is adding a very important feature to the design [16]. With this feature, the device can keep regulating the desired 280V output voltage even if there are voltage drops on the input DC bus. While a step-up converter would normally be required to add such a feature to the design, the inherent characteristics of the LLC topology enable this requirement to be achieved without any additional components.

For these reasons, the wide and flexible gain range and inherent boosting properties of the LLC topology make it a technically superior option for battery charging applications.

CHAPTER IV
GENERAL SYSTEM ARCHITECTURE AND BLOCK DIAGRAM

4.1 A CHARGER AS A FUNCTIONAL WHOLE

In the previous sections, the fundamental objectives, electrical, and physical requirements for the charger to be developed were defined, and the LLC Resonant Converter was selected as the most suitable power topology to achieve these objectives. This section presents how this selected topology and all other auxiliary subsystems are integrated to form a functional whole, i.e., the overall system architecture.

This architecture constitutes the main plan of the project and defines all fundamental interactions, such as power flow, control signal flow, sensing mechanisms, and communication interfaces. The presented block diagrams aim to break the system down into more understandable functional units, clarifying the role of each unit and its place in the overall system operation. This plan serves as a roadmap for the design processes detailed in the following sections.

4.2 HIGH LEVEL FUNCTIONAL BLOCK DIAGRAM

The complete architecture of the charger consists of several main functional blocks that work together in an integrated manner. Figure 3 shows these blocks and the essential power and signal flow between them.

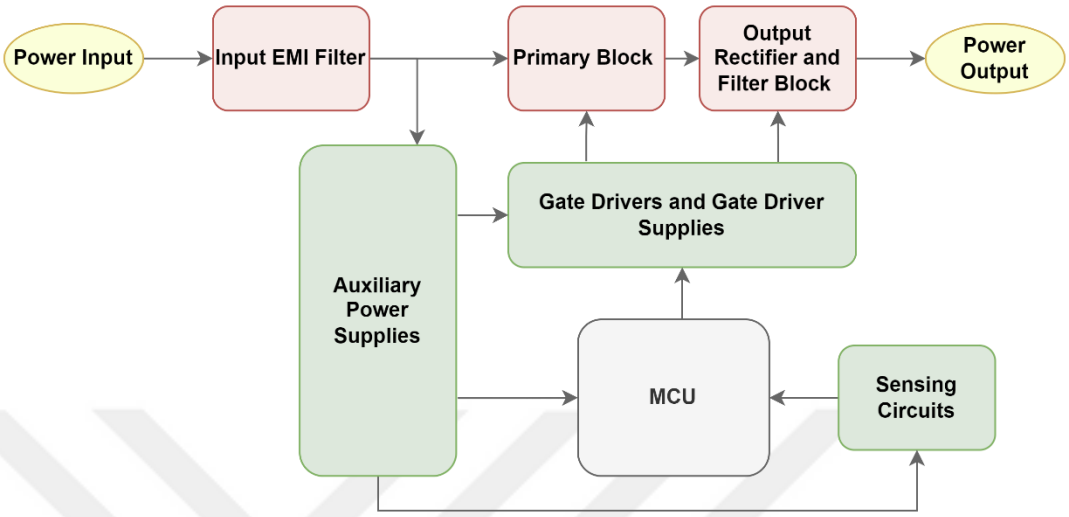

Figure 3: General System Block Diagram

The function of each block in the system architecture presented above is described below:

- **Input EMI Filter:** This is the first functional block of the system's power stage. It filters noise that may come from the 270VDC bus while also preventing the switching noise generated by the converter from leaking back into the bus. Additionally, it contains the initial protection circuits (fuses, TVS diodes, etc.) against overcurrent and overvoltage. This layer, which is a prerequisite for almost all electrical avionics equipment, is where many requirements are met. A detailed EMI analysis and EMI filter design will not be the subject of this thesis.
- **Primary Block:** This is one of the main blocks that constitutes the core topic of the thesis. It houses the primary side of the selected LLC resonant topology. It converts the high DC voltage into a high-frequency AC voltage. Subsequently, through a transformer, it provides galvanic isolation and transfers the high-power AC voltage to the secondary side.
- **Output Rectifier and Filter Block:** This block converts the high-frequency AC voltage from the secondary side of the transformer back into DC to charge the battery. To increase efficiency, it uses either ultrafast diodes or, preferably,

FETs that perform synchronous rectification (SR). Output capacitors minimize the ripple in the DC voltage.

- **MCU Block:** This is the central control unit of the system. It makes all the decisions. It's the brain, executing all the sensing, calculating, and control functions. It constantly watches over the output voltage and current, following the CC-CV charging algorithm, and intelligently adjusting the switching frequency with PFM. Otherwise, it manages any unexpected issues or faults and keeps a clear line of communication open with the other units.
- **Sensing Circuits:** These are the circuits that reduce and/or filter analog quantities, such as output voltage, output current, and temperatures at critical points, to voltage levels that the controller can process.
- **Gate Driver and Gate Driver Supplies:** This block converts low-power PWM signals from the controller into high-current signals that can quickly and effectively switch the power FETs on and off. In isolated converters, versions that provide isolation between the primary and secondary sides are used.
- **Auxiliary Power Supplies:** These are the power supplies that generate the stable voltages required for the controller, drivers, and other low-voltage integrated circuits from the high-voltage 270V DC bus.

4.2.1 Power Stage Flow Architecture

The power flow architecture defines the system's fundamental task of transferring energy from one point to another.

Figure 4 provides a simplified view, showing only the path the power takes.

Figure 4: Power Stage Flow Architecture

Energy is taken from the 270VDC busbar and first converted into a high-frequency square-wave voltage by full-bridge FET switches. The resonance tank is powered by this square wave, which mainly determines the efficiency and control features of the system. The energy is therefore sent to the secondary side through a high-frequency transformer that offers galvanic isolation. On the secondary side, synchronous rectifier FETs are employed to make the conversion of this high-frequency AC into DC. Finally, the pure DC energy that constitutes the charging source of the battery pack is enabled by the output capacitors that have been used for the filtering process [23].

4.2.2 Control and Data Flow Architecture

The control and data flow architecture is what guarantees the safe and proper management of power flow. This framework is the system's brain which makes the decisions.

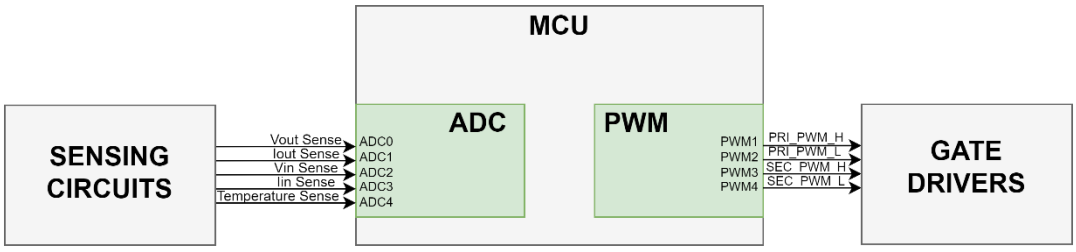

Figure 5: Control and Data Flow Architecture

Control operation starts with sensing circuits that sense the output voltage and current. This analog data is converted into digital values by ADCs within the MCU. The core software within the MCU uses this data to run the CC-CV algorithm and calculate the required switching frequency instantly. This calculation is loaded into the high-resolution PWM hardware unit, which generates the PWM signals that drive the primary-side switches.

CHAPTER V
ANALYSIS AND DESIGN OF THE LLC RESONANT CONVERTER

In the previous section, the requirements were determined, and a general block diagram of the charger was generated based on these requirements. It was also stated that the Full Bridge LLC topology was selected based on these requirements. This section will discuss the structure, operating logic, and design approach of this topology in detail.

5.1 INTRODUCTION TO LLC RESONANT POWER CONVERSION

Today, the ever-increasing demand for efficiency and power density in power electronics applications encourages the use of more advanced solutions to replace conventional PWM-based converter topologies[20], [21]. For this reason, resonant-based converters are often preferred, especially due to their high efficiency, low loss, small-sized passive elements, and soft switching capability. Among these resonant topologies, the LLC resonant power converter has become the preferred choice due to its ability to adapt to a wide input/output voltage range and to operate with low loss at high switching frequencies.

5.2 GENERAL STRUCTURE OF LLC RESONANT CONVERTER

5.2.1 Primary-Side Bridge Inverter

In LLC resonant converters, the input stage is typically a half-bridge or a full-bridge. The half-bridge uses two power switches, while the full-bridge uses four. The choice depends on the application and required power. For high-power designs of about 1000 W and above, the full-bridge is generally preferred [24].

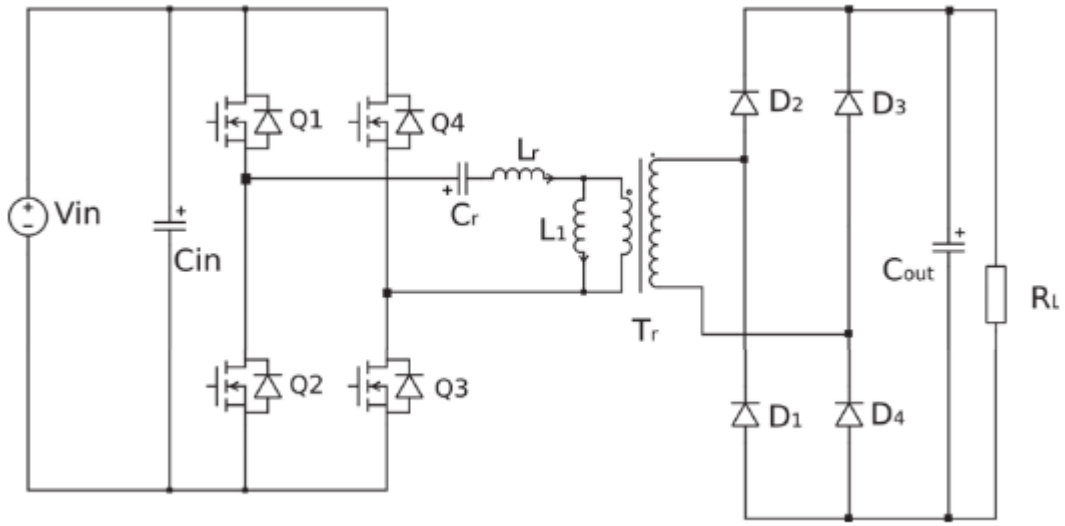

Figure 6: Full Bridge LLC Converter Topology [4]

The switches Q1 and Q3, along with Q2 and Q4, are turned on and off in a complementary manner to create a square-wave voltage. These switches are typically driven at a fixed 50% duty cycle. A small dead-time is usually added between the complementary pairs' switching to prevent cross-conduction and ensure zero voltage switching (ZVS) [4].

5.2.2 Resonant Tank

The resonant tank is made up of a resonant capacitor (Cr) and two inductors: the series resonant inductor (Lr) and the transformer's magnetizing inductor (Lm). When the switching H-bridge applies a square-wave voltage to this tank, it generates a resonant sinusoidal current. The transformer then steps this current up or down [4].

Lr is the main resonant current path of the circuit. Often, the transformer's leakage inductance can serve this purpose. Alternatively, if the converter is designed with a planar transformer, an external inductor is added to achieve the desired value.

The magnetizing inductance (Lm) is the inductance associated with the transformer. It is the main responsible for keeping the switching smooth, switching performed under light load conditions, especially. The Lm value is very important to ensure the LLC topology works efficiently and stable not only under light load conditions but also under high load conditions. This is because at lower loads the resonance frequencies of Lm+Lr and Cr are approached on the LLC gain curve [17]. At higher loads, the resonance frequencies of Lr and Cr are approached on the gain

curve [17]. The gain at the resonance frequency is always 1 and it is not affected by load changes. Moreover, this converter can be used as a step-up as well as a step-down mode [17].

$$f_r = \frac{1}{(2 * \pi * \sqrt{L_r * C_r})} \tag{5.1}$$

$$f_1 = \frac{1}{(2 * \pi * \sqrt{(L_r + L_m) * C_r})} \tag{5.2}$$

The series resonant frequency (fr) is defined by the resonant capacitor (Cr) and Lr. Besides that, the parallel resonant frequency (f1) is generated when Lm is connected [17]. This double resonant feature is what makes the LLC capable of a wide output voltage range

The choice of the resonant tank elements (Lr, Lm, and Cr) is most often a complex multi-variable optimization problem, as it involves figuring out three interdependent variables simultaneously [23]. Consequently, it is recommended to employ sophisticated simulation software during the designing stage to work up and examine different operating points and gain curves [23]. The best design point is chosen from these curves with reference to the load range and efficiency intended. The basic parameters such as Lr, Lm , and Cr are then figured out from this point [23]. By means of this method it becomes possible to achieve soft-switching conditions and to optimize the operating frequency and gain values of the converter [23].

5.3 RESONANT TANK EQUATIONS AND DESIGN FLOW CHART

After figuring out the needs and the different circuit structures for the LLC resonant converter, it is necessary to find the minimum and maximum gain values from those requirements. These figures will significantly influence the both the transformer design and the choice of the resonant tank components.

Consequently, the transformer ratio is established in line with the input and output requirements. Usually, this ratio is dependent on the connection between the standard input and output voltages [25].

$$n = \frac{Vout_{nom}}{Vin_{nom}} \tag{5.3}$$

Next in our design, we want to figure out what the maximum Quality Factor (Q) could be. We will begin by looking the expression for Q in LLC topology. The formulas for Q and its constituent variables are provided below.

$$Q = \frac{\sqrt{\frac{L_r}{C_r}}}{R_{ac}} \tag{5.4}$$

$$R_{ac} = \frac{8}{\pi^2} * \frac{N_p^2}{N_s^2} * R_o \tag{5.5}$$

As seen, the reflected load resistance (Rac) is a variable influenced by the output load (Ro). Therefore, it is correct to make a selection based on the maximum load at which the system will operate.

After determining the maximum Quality Factor (Q), we need to continue the design by selecting the values for the transformer's primary inductance and the resonant inductance. The relationship between these two values is called 'm', or the Ratio of total primary inductance to resonant inductance. The value of 'm' is another variable that defines the gain curve of the design. Its formula is given below.

$$m = \frac{L_r + L_m}{L_r} \tag{5.6}$$

When a low 'm' value is chosen, the gain curve becomes more flexible. This allows for a wider gain curve with a narrower frequency range. However, a low 'm' value also has its disadvantages [23]. For the same Q and fr, choosing a low 'm' value means that the magnetizing inductance (Lm) will also be lower [23]. The lower the value of Lm, the greater the peak-to-peak ripple current, hence conduction losses increase, reducing the efficiency in the converter [23].

When a high value of 'm' is chosen, a narrow gain curve is presented [23]. This can be difficult as the frequency may have to be drastically increased to provide lower voltages [23]. Although ZVS is maintained, a higher frequency practically results in increasing switching losses.

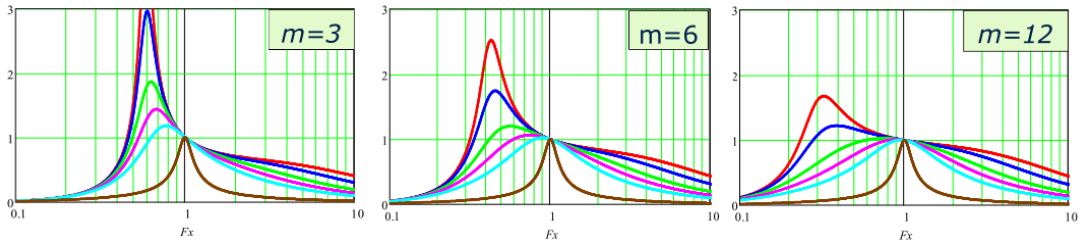

Figure 7: Comparing LLC Gain at Different 'm' Values [23]

For these reasons, the choice of the value of 'm' is very critical. In order to ensure that the most appropriate gain value is chosen for the application in hand, it is useful to plot and compare the gain curves for various different 'm' values. Once a choice is made, it will play a critical role in validating the design and selection to verify the value with a SPICE simulation.

The equation used to plot the gain curves is:

$$K = \frac{F_x^2 * (m-1)}{\sqrt{(m * F_x^2 - 1)^2 + F_x^2 * (F_x^2 - 1)^2 * (m-1)^2 * Q^2}} \tag{5.7}$$

Based on the gain equation above, gain curves will be created. Fx is defined as the normalized switching frequency, which is the ratio of the switching frequency to the resonant frequency.

$$F_x = \frac{f_s}{f_r} \tag{5.9}$$

Now that we have our gain curves for different values of m and Q, we will need to choose our resonant frequency by comparing these curves with our requirements. The resonant frequency chosen will affect both the size and the value of the passive elements to be used in the design. Choosing too high a frequency can increase the power density by choosing smaller materials. However, it is important to set a limit to the maximum frequency in order to keep switching losses to a minimum and to fine-tune the sensitivity of the modulation.

Now that we have a lot of inputs, we can use the equations of Q and fr to determine the values of Lr and Cr and solve these two equations jointly.

A flowchart that summarizes and aggregates what I have explained above is shared below.

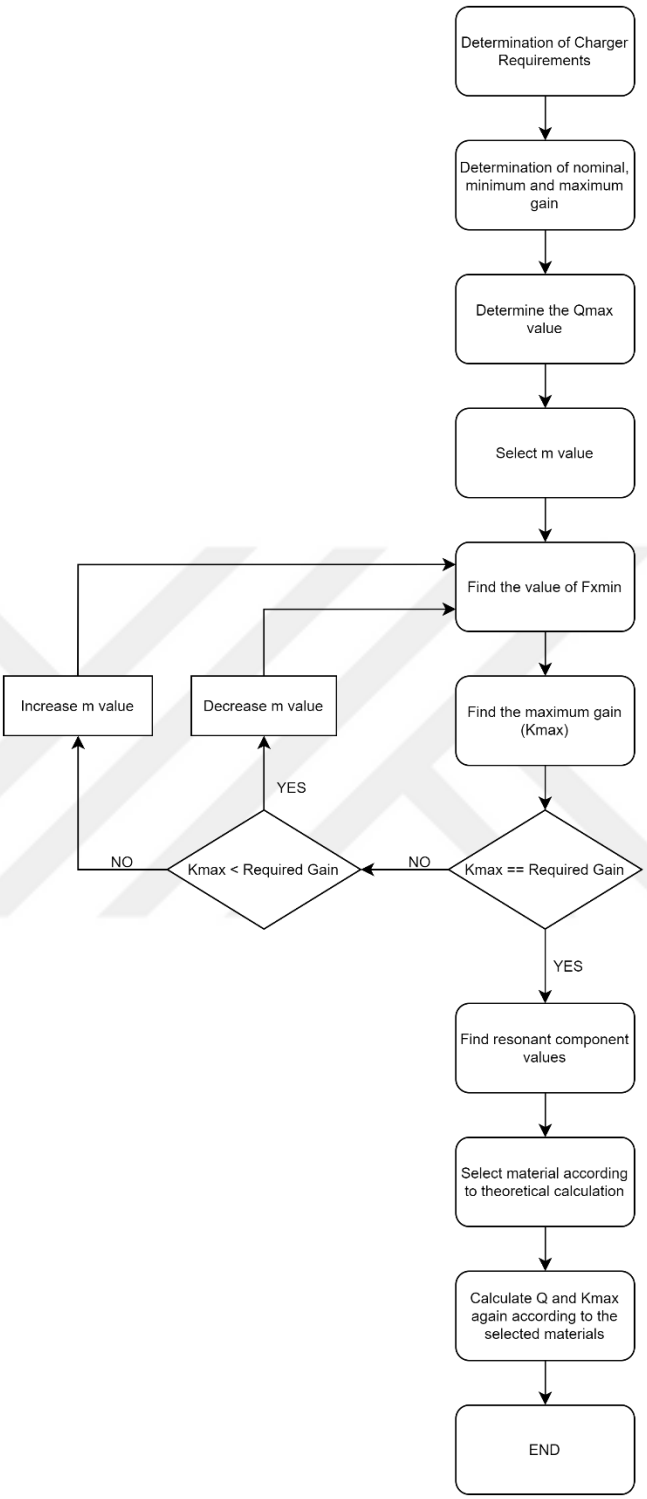

Figure 8: LLC Converter or Charger Design Flowchart

5.4 RESONANT TANK DESIGN & PARAMETER CALCULATION

In this section, theoretical calculations for charger design will be made using the formulas given in the previous section and the flow chart.

5.4.1 Determining the Minimum and Maximum Gain

According to the requirements specified in Table 1

Maximum Gain:

$$K_{max} = \frac{Vout_{max}}{Vin_{min}} = \frac{280}{240} = 1.1458 \tag{5.10}$$

Minimum Gain:

$$K_{min} = \frac{Vout_{min}}{Vin_{max}} = \frac{230}{275} = 0.8363 \tag{5.11}$$

Now that these two values are known, we can draw gain curves for different values of Q and m and advance our design according to the curve that suits us.

5.4.2 Calculation and Selection of m, Q, and Rac Values

In order to advance the design, it is first necessary to select an initial value of m. This value will be used to compare the gain curves, and if it is suitable, it will be selected directly. If it is not found to be a suitable value in the comparison of the curves, it will be increased and decreased until a suitable gain curve is found. The initial value of m is selected below.

$$m = \frac{L_r + L_m}{L_r} = 6 \tag{5.12}$$

Now, according to this selected value, the gain curve can be plotted for different Q values.

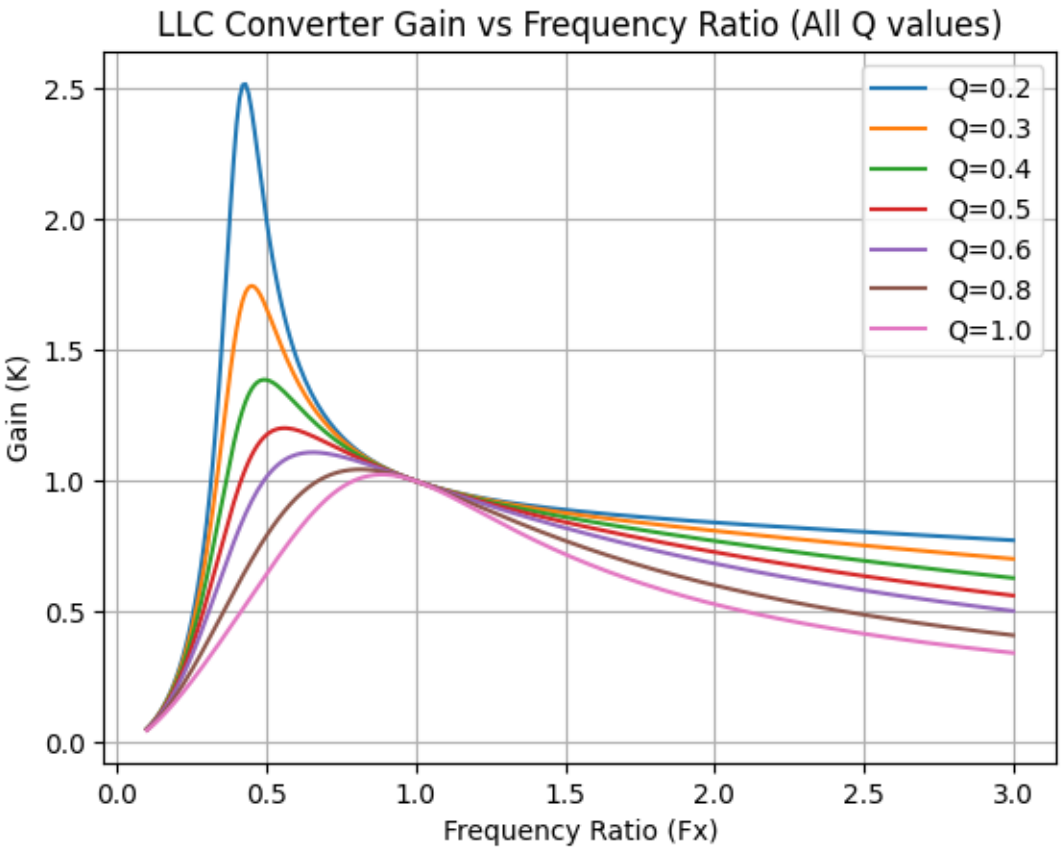

Figure 9: LLC Converter Gain vs Frequency Ratio (All Q Values)

After the Q curves are plotted, the most appropriate Qmax value is selected according to the minimum gain and maximum gain values.

When the selected values are compared, it is evaluated that the Qmax = 0.5 value may be suitable for us.

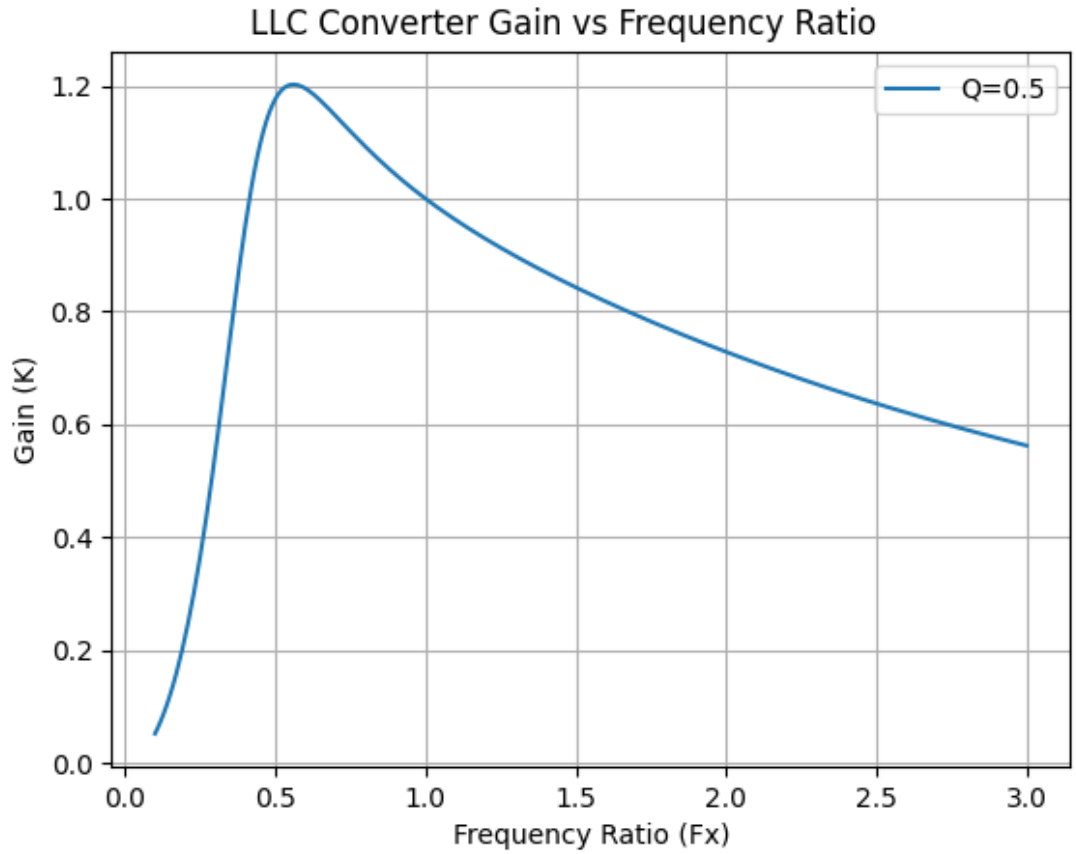

Figure 10: LLC Converter Gain vs Frequency Ratio (Q = 0.5)

Since the Q value varies according to the load, the maximum value of Q selected in this section is the maximum value of Q [23]. This Qmax value can be deceptive if the system is expected to reduce gain at half load or light load. It may not be appropriate to design inverters with very wide input or output ranges using LLC or similar resonant inverters. The main purpose here is to determine an operating frequency range and to ensure that it operates with the highest efficiency and minimum loss in this range. A gain curve that varies according to the load may mislead us when determining this range.

Now we will calculate the Rac value used in the formula of Q. After calculating this value, there will be no obstacle in front of us to find the values of Lr and Cr.

$$R_{ac} = \frac{8}{\pi^2} * \frac{N_p^2}{N_s^2} * R_o = \frac{8}{\pi^2} * \frac{N_p^2}{N_s^2} * \frac{V_o^2}{P_o} = \frac{8}{\pi^2} * \frac{1}{1} * \frac{270^2}{1800} = 34.76 \qquad (5.13)$$

5.4.3 Selection of Resonant Frequency

The selection of the resonant frequency is a matter that will shape the entire design. Selecting a high frequency may allow for:

- Smaller Lr and Cr selections.
- Smaller transformer selections.
- Smaller output capacitors.

However, the same selection has some disadvantages:

- Although LLC resonant converters have low switching losses thanks to ZVS, this does not mean that the loss is zero. Especially when operating at frequencies different from the resonant frequency, these losses increase significantly. ZVS begins to degrade.
- The power consumption of the FET drivers increases. This situation will eventually cause the drivers to overheat. In aviation-qualified products, environmental conditions are harsh, and operation at high temperatures is expected. Overheating of the drivers can cause them to thermal shutdown, and worse, cause damage.
- If you are building a digitally controlled converter, the resolution of the MCU used determines the limits of the converter. To achieve very high frequencies, a more powerful MCU is required. However, there are limits to the processors available on the market. Pushing this resolution limit too far can make it difficult to set the desired frequency and deadband value.

5.4.4 Calculation of Lr Cr and Lm Values

When designing a resonant tank, we can find the Cr and Lr formulas by solving the Q and fr formulas together.

$$C_r = \frac{1}{2 * \pi * Q_{max} * f_r * R_{ac}} = 68\ nF \tag{5.14}$$

$$L_r = \frac{1}{(2 * \pi * f_r)^2 * C_r} = 24\ uH \tag{5.15}$$

$$L_m = (m - 1) * L_r = (6 - 1) * 24\ uH = 120\ uH \tag{5.16}$$

Based on theoretical calculations, we have determined the parameters of our resonant tank. Now we will select the appropriate components.

5.4.5 Selection of Cr Components

In resonant capacitor selection, it is more appropriate and safer to choose film capacitors for this type of application. Polypropylene film capacitors are frequently preferred and used for this type of application [26]. Their high-frequency operating characteristics, high current capacities, and AC and DC high-voltage capacities make them suitable for this design.

In this application, the Double Metallized Polypropylene Film type R76TI218050H4J capacitor has been selected. Four of these 18nH capacitors will be used in parallel. Parallel use is important in such applications, both to reduce the effect of capacitance tolerance and to divide the current passing through the passive element.

The R76TI218050H4J product stands out with its high temperature ratings. Using high-spec products is important in aviation applications. The rigorous tests that will be performed during product verification necessitate the selection of high-quality, high-spec products.

If we examine the product's specifications below, the 650 VAC voltage capacity will be sufficient for us. The product's AEC-Q200 qualification also indicates that it has passed certain tests and proven itself under harsh conditions.

Specifications	
Capacitance	0.018 uF
Tolerance	5%
Voltage DC	1600 VDC
Voltage AC	650 VAC
Temperature Range	-55/+125°C
Rated Temperature	105°C
Dissipation Factor	0.03% 1kHz, 0.04% 10kHz, 0.1% 100kHz
Insulation Resistance	100 GOhms
Max dV/dt	6,000 V/us
ESR	35.37 mOhms (100kHz)
Ripple Current	2.93 Amps (100kHz 100C), 108 Amps (Peak)
Inductance	10 nH

General Information	
Series	R76H
Dielectric	Double Metallized Polypropylene
Style	Radial
Features	Automotive Grade, Pulse
RoHS	Yes
Termination	Tinned Wire
Lead	Wire Leads
Qualifications	AEC-Q200
AEC-Q200	Yes
Typical Component Weight	2.47 g

Figure 11: R76TI218050H4J Specifications

Furthermore, when we examine the graphs provided in the product datasheet below, we see that the product will continue to perform without any deviation or derating within our operating frequency range.

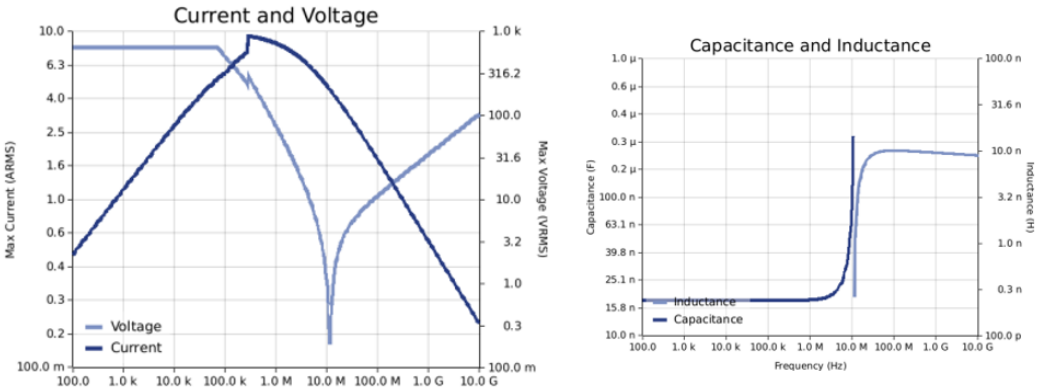

Figure 12: R76TI218050H4J Frequency Response

Four parallel uses of the product will give us a capacity of 72nF. This value is close to the calculated value. The minor disparities between the theoretical computation and the practical choice will not considerably change the design regarding the alterations of the resonant frequency and the changes in the Qmax calculation.

5.4.6 Selection of Lr Components

A planar transformer was used in this design to satisfy the goals of high power density and system optimization. As a result of the low leakage inductance inherent in planar transformers, and also the design flexibility given by the integration of an external inductor, it was decided to implement the resonant inductance (Lr) as a separate component. This part is dedicated to the explanation of the external resonant inductor design, which was aimed at attaining 22 µH value.

The main purpose of the resonant inductor design is to supply the necessary inductance and at the same time limit the total power losses to a minimum under conditions of high resonant current. The total power loss in an inductor is made up of two main components: copper loss that is the one occurring in the windings, and core loss (Pcore), which is the loss arising in the magnetic core. An efficient design intends to put a compromise between these two losses mechanisms.

5.4.6.1 Design Methodology and Loss Calculations

Usually, inductor design is an iterative process that starts with the pick of suitable core geometry and material. After selecting the core, the core and copper losses are estimated from the theory. In case the sum of losses and consequent temperature rise are beyond the set target values, the whole process is repeated by either choosing a bigger core or another material.

5.4.6.1.1 Core Loss Analysis

Core loss includes hysteresis and eddy current losses, these both come from the switching frequency and changes in magnetic flux density. The calculation of it is more complicated than that of copper loss and it needs the determination of peak magnetic flux density first. The current in the resonant tank of the LLC converter is a pure AC sinusoidal current without any DC component. Here, the peak magnetic flux density is determined by the following formula:

$$B_{pk} = \frac{L_r * I_{pk}}{N * A_e} \tag{5.17}$$

Where Lr is the required inductance, Ipk the peak value of the resonant current, N the number of turns, and Ae the effective cross-sectional area of the chosen core.

After that, the core loss density (Pv, usually in mW/cm³) corresponding to the Bpk value can be found by calculating with the coefficients given by the manufacturer for the used core material. The calculation is done via the Generalized Steinmetz Equation (GSE).

$$P_v = k * f_s^{\alpha} * B_{pk}^{\beta} \tag{5.18}$$

Here, f is the switching frequency, and k, α, and β are the Steinmetz coefficients for the core material. The total core loss is, in the end, figured out by multiplying the loss density by the effective core volume (Ve) which has been calculated.

$$P_{core} = P_v * Ve \tag{5.19}$$

5.4.6.2 Copper Loss Analysis

Copper loss represents the ohmic loss that is incurred as the RMS current passes through the winding resistance. It is estimated after the core and number of turns are decided upon because it is then that the winding resistance will change based on the number of turns and the conductor properties.

$$P_{cu} = I_{rms}^2 * R_{DC} \tag{5.20}$$

5.4.6.3 Final Design and Parameters

Table 2 summarizes the parameters for the final inductor design that guarantees the desired electrical and thermal performance based on the chosen core geometry and material as a result of the iterative design process described above. The loss calculation using the Steinmetz equation will be done from these final parameters.

Table 2: Resonant Inductor Design Parameter

Parameter	Requirement
Inductance (Lr)	22uH
Avarage Frequency	150 kHz
Peak current amplitude (Ipk)	12.5 A
RMS current (Irms)	8.7 A
A_e	165mm^2
l_e	5.6 cm
V_e	10.224 cm^3
$A_{L,ungap}$	8100
$A_{L,gap}$	153
k	92.6
α	1.54
β	2.78
DCR	0.026

By using these parameters, the in-depth loss analysis will provide a quantitative measure of the designed resonant inductor's contribution to the total efficiency and thermal performance of the system.

5.4.6.4 Core Selection and Critical Role of Air Gap

The initial and quite essential step in the design of an inductor is the choosing of the right magnetic core. One of the main features of the inductor is that it has to

keep its magnetic properties, even at a high peak current of 12.5 A, which implies that the magnetic core should not be saturated.

Essentially, a typical magnetic core comes in two main forms: ungapped and gapped. The variances of their inductance factor values make this decision most influential in energy storage applications.

- **Ungapped Core:** ~8100 nH/N². This high A_L value indicates that a large inductance can be achieved with only a few turns. However, such a structure reaches magnetic saturation even at relatively low current levels.
- **Gapped Core:** ~153 nH/N². By intentionally introducing an air gap into the magnetic path of the core, the A_L value is drastically reduced. This air gap increases the effective magnetic reluctance of the core, allowing it to tolerate much higher peak currents without reaching saturation and, as a result, enabling it to store significantly more energy.

Since the primary role of the resonant inductor in this charger is to store and transfer energy under high current conditions, the use of a gapped core is essential. Therefore, all subsequent calculations have been carried out based on the $A_{L,gapped}$ value of the gapped core.

5.4.6.5 Loss of Inductor

Using the gapped AL value of the selected core, the number of turns required to achieve the target inductance of 22 µH is calculated.

$$N = \sqrt{\frac{L_r}{A_{L,gap}}} = \sqrt{\frac{22 * 10^{-6}\ H}{153 * 10^{-9}\ H/N^2}} = 12 \tag{5.21}$$

Using the determined number of turns, the maximum magnetic flux density in the core is calculated at the peak current of **12.5 A**.

$$B_{pk} = \frac{22 * 10^{-6}\ H * 12.5\ A}{12 * 165 * 10^{-6}\ m^2} = 0.139\ T \tag{5.22}$$

The total core loss is calculated using the Generalized Steinmetz Equation (GSE).

$$P_{core} = 92.6 * (150 * 10^3 Hz)^{1.54} * (0.139\ T)^{2.78} * (10.224\ cm^3) \quad (5.23)$$

$$P_{core} = 1.92\ W \quad (5.24)$$

The theoretically calculated core loss remains at an acceptable level for the progress of the design.

Finally, the copper loss is calculated as outlined below, completing the overall design analysis.

$$P_{cu} = (8.7A)^2 * 0.026 = 1.97 \quad (5.25)$$

5.4.7 Calculation of Current Q and fr Based on Lr and Cr Selections

The resonance frequency (fr) and quality factor (Q), which determine the gain characteristics of the LLC converter and form the starting point for the design, are directly related to the resonance tank components Lr and Cr. During the theoretical design phase, ideal values for these components are calculated to achieve the desired performance. However, in practice, it is often not possible to find components with these ideal values on the market. Instead, the closest values are selected from inductors and capacitors manufactured with specific nominal values.

Selected Resonance Tank Values:

- Lr = 22 uH,
- Cr = 72 nF

With these selected practical component values, it is necessary to recalculate the system parameters fr and Qmax.

The resonance frequency is directly dependent on the Lr and Cr values. It has been recalculated.

$$f_r = \frac{1}{(2 * \pi * \sqrt{22uH * 72nF})} = 126500\ Hz \quad (5.26)$$

In all subsequent analyses, the value of 126.5 kHz will be used as the reference for the system's actual resonance point.

The quality factor (Q) value is another parameter affected by these selections. The value Q serves the function of the converter gain curve. So, it is the shape that

depends on the Q value. Therefore, one needs to recalculate it in accordance with the parameters that have been finally chosen.

$$Q = \frac{\sqrt{\frac{L_r}{C_r}}}{R_{ac}} = \frac{\sqrt{\frac{22uH}{72nF}}}{34.76} = 0.5 \quad (5.27)$$

The latest elections reveal that our previously determined Q value has remained unchanged, and the value is 0.5.

5.5 PLANAR TRANSFORMER SELECTION & OPTIMIZATION

5.5.1 High Frequency LLC Transformer Overview

In LLC resonant converters, the high-frequency transformer plays a key role in ensuring the efficient operation and compact design of the converter. This transformer not only converts between input and output voltage levels but also provides galvanic isolation. In LLC converters, the transformer's leakage inductance is typically used as the resonant tank's inductance. However, if a planar transformer is used, this must be achieved using an external inductor with an Lr value. Attempting to add leakage inductance to a planar transformer would increase the design and production costs of the transformer.

Planar transformers are becoming increasingly common in LLC converters compared to classic cylindrical wound designs. Planar transformers offer a lower profile, better heat dissipation, less leakage inductance, and better electromagnetic compatibility thanks to their multi-layer PCB structures. They also offer advantages in terms of automation and mechanical durability in production [27].

A planar transformer structure will be preferred in this design. The advantages of this are as follows.

- High power density.
- Easy thermal management.

Planar transformers will help us increase the power density of an avionics charger with their regular geometric shapes and low volume. They will also provide a great advantage for cooling by easily contacting the cooling surface.

5.5.2 Planar Transformer Calculation and Analysis

The first parameter to be determined in transformer design and/or selection is the transformer ratio.

$$n = \frac{N_p}{N_s} = \frac{K_{min} * Vin_{max}}{Vout_{min}} = \frac{0.8363 * 275}{230} = 1 \quad (5.28)$$

After calculating the transformer ratio using minimum gain, another value is the Lm value of the transformer. This value can be calculated automatically after determining the Lr and m values.

When selecting the core, it is important to keep transformer loss to a minimum. When designing a full-bridge converter, the Bmax value is calculated as follows.

$$B_{max} = \frac{2 * Vin_{max}}{4 * N_p * Ae * f_s} \quad (5.29)$$

Bmax (Peak Flex Density) is one of the factors that determines core loss. Core loss is calculated as follows.

$$P_{core} = k * f_s^{\alpha} * B_{pk}^{\beta} * Ve \quad (5.30)$$

The Pcore equation is important for core selection. We will perform this calculation for the cores we can choose from and try to arrive at the most optimal selection.

The coefficients for DMR95, the material I chose for this design, are shared below.

- k = 92.17
- α = 1.045
- β = 2.44

After many iterations, the parameters of the selected kernel are shared below.

- $Ae = 530mm^2$
- $Ve = 49.22cm^3$

If we calculate Bmax and Pcore based on the above values

$$B_{max} = \frac{2 * Vin_{max}}{4 * N_p * Ae * f_s} = \frac{2 * 275V}{4 * 16 * 530mm^2 * 125kHz} = 108mT \quad (5.31)$$

$$P_{core} = 92.17 * 150kHz^{1.045} * 108mT^{2.44} * 49.22cm^3 = 3.74\,W \quad (5.32)$$

The loss value of 3.74 watts will not cause us any difficulty in cooling a core of this size. Considering that the design will include both a heatsink and a fan to cool the heatsink, this value can be easily cooled.

Finally, since the "m" value is selected as 6, the Lm value of the transformer can be calculated as follows.

$$L_m = (m-1) * L_r = 5 * 22uH = 110uH \quad (5.33)$$

5.6 SEMICONDUCTOR DEVICE (FET/SIC) SELECTION

The selection of switching elements is another critical issue for converters. SICFETs stand out in this selection with their high voltage capacity, high current capacity, and low Rdson option. SICFETs can provide VDS voltages of 650V and above with low Rdson.

After reviewing many SICFETs, the product that was selected is the NVBG032N065M3S.

The product specifications are listed below.

Table 3: NVBG032N065M3S Parameters

Parameters	**Values**	**Meanings**
VDS	650 VDC	An input voltage more than twice the specified value will ensure that the FET operates safely even during transient voltage surges.
Rdson	32 mΩ	A low Rdson value will minimize transmission losses on both the primary and secondary sides.
Qg	55 nC	A low gate charge value will reduce the current drawn from the gate driver. This will prevent temperature increases in the gate driver circuits.
Id	52 A	It is significantly higher than the input and output current to be drawn.

Another feature of the product is the presence of a kelvin-source leg. This leg makes the differential gate-source line drawing more meaningful in the PCB design.

As a result, gate source lines with less parasitic inductance and capacitance will minimize high voltage fluctuations that may occur on the switched gate source voltage.

The product is an H²PAK 7 SMD package product. The SMD nature of the product will facilitate PCB placement. In addition, when creating a surface for the heatsink, it will allow us to create a cooling surface on the other side of the board with vias.

5.7 OUTPUT RECTIFICATION

5.7.1 Design Considerations for High-Efficiency Rectification

The high frequency alternating current (AC) power generated on the primary side of the LLC converter and transferred to the secondary side via the transformer must be converted back into a stable direct current (DC) to charge the battery pack. This process is performed by the output rectifier stage.

The rectification process is divided into two types: passive rectification and active rectification.

- **Passive Rectification:** This is the simplest rectification method. It is performed using ultra-fast SIC or Schottky diodes. Diodes are advantageous because they do not require control and are simple. However, they have a fixed forward voltage drop (Vf) when current flows through them. At high currents, this voltage drop can exceed 1V. In this case, the loss across the diodes increases significantly. For example, when passive rectification is performed according to the following formula, the transmission loss is calculated as 6W by selecting a nominal diode voltage of 1V. This loss causes a reduction in power density [28].

$$P_{loss} = V_f * I_{out} = 1V * 6A = 6W \quad (5.34)$$

- **Active Rectification:** In this method, instead of diodes, power FETs with very low resistance (Rds(on)) when conducting are used. These FETs are turned on and off at the right moments by a controller so that they behave like diodes. For example, when a FET with Rds_on = 0.02Ω is used, the conduction loss is calculated as follows [28].

$$P_{loss} = R_{ds(on)} * I_{out}^2 = 0.02\Omega * (6A)^2 = 0.72W \quad (5.35)$$

This simple comparison clearly shows that the use of the Synchronous Alignment (SR) method is essential to achieve the targeted high efficiency.

5.7.2 Rectifier Architecture Selection

Two basic architectures stand out for synchronous rectification applications: Center-Tap and Full-Bridge.

- **Center-Tap Architecture:** Although it requires two FETs, it creates twice the output voltage stress on the FET that is not conducting. This necessitates the use of FETs that are more resistant to higher voltages and therefore have higher Rds(on) values. Additionally, the difficulty of creating a symmetrical center-tap winding in a planar transformer structure is another disadvantage of this architecture.
- **Full-Bridge Architecture:** Although it uses four FETs, it reduces the voltage stress on each FET to the output voltage level. This critical advantage allows for the selection of low-voltage FETs with ultra-low Rds(on) values, enabling significantly superior performance.

In this thesis, the Full-Bridge Architecture is used on the secondary side. Using the same structure on both the secondary and primary sides in a digitally controlled converter will facilitate Synchronous Rectification. This is because in LLC converters, if the switching frequency is greater than or equal to the resonant frequency, the drive signals can operate synchronously with the primary switches [29].

5.8 OPERATING MODES OF LLC RESONANT CONVERTER

5.8.1 Operation at Resonance (*fs = fr*)

Operation at the resonant frequency represents the nominal design point of the LLC converter. At this point, the resonant tank operates in perfect synchronization with the primary-side switching frequency. In this mode, each switching half-cycle precisely corresponds to a full resonant half-cycle [23]. Consequently, the resonant current (ILr) naturally returns to zero as the complementary switch branch turns on [23].

This synchronous behavior provides optimal switching conditions for all

semiconductor elements [23]. The primary-side FETs perform near-lossless Zero Voltage Switching (ZVS), where the tank current creates the conditions necessary for the switch voltage to drop to zero before turning on. Simultaneously, the secondary-side rectifiers naturally commute using Zero Current Switching (ZCS), which eliminates reverse recovery losses, a major problem in hard-switched topologies.

At this specific frequency, the voltage gain of the power stage is essentially unity. Therefore, the transformer's winding ratio is deliberately selected to meet the nominal input and output voltage requirements, so that no step-down or step-up action is required under these ideal conditions. Consequently, operation at resonance offers the highest possible efficiency and places the lowest voltage and current stress on the components.

5.8.2 Operation above resonance (fs > fr)

When the input bar voltage rises toward its upper limit or a lower output power is required, the controller weakens the voltage gain by raising the switching frequency above the resonance frequency in order to maintain regulation. In this operating region, the switching period becomes shorter than the natural resonance period of the tank [23].

This causes each resonant half-cycle to be prematurely terminated by the next switching event before it can complete its natural sinusoidal path [23]. Consequently, the secondary-side rectifiers are forced to turn off while current continues to flow, leading to the loss of ZCS and a condition known as "hard commutation"[23]. As a result, the are reverse-recovery losses introduced and the secondary elements are being heavily stressed [23].

At this point, the tank voltage gain of the circuit falls below one, thus, the converter acts as a buck stage. The attribute in question is basically the fundamental feature of the controller that stops it from going beyond the output voltage setpoint under the condition of a high input voltage. Although ZCS loss causes a slight decrease in the total efficiency, Zero Voltage Switching (ZVS), which is very important to the primary-side FETs, is still very strong as the tank energy is still enough to discharge the device capacitances during the dead time [23].

5.8.3 Operation below resonance (fs < fr)

When there is a low input voltage or the output power is high, the controller lowers the switching frequency below the resonant frequency to increase the voltage. The induction region of the operation is such that the switching period is longer than the resonant period [23].

Once the power transfer through the main interval is over, the resonant tank is basically short-circuited by the primary-side switches for the rest of the half-cycle [23]. As a result, a huge circulating current is flowing through the primary circuit, which does not produce output power but, however, greatly increases the RMS current [23]. Such an increased current worsens the conduction losses in the FETs and transformer windings, which losses are proportional to the current squared [23].

Still, this huge circulating current - while it narrows the ZVS window and thus requires the dead time and inductance ratio to be adjusted carefully - quite firmly ensures ZVS in all conditions [23]. Since the voltage gain is higher than one, the converter is thus operating as a step-up stage, which is a way of ensuring that the battery will be able to be fully charged even if the input voltage decreases. Due to high circulating currents, this mode of operation represents the worst-case thermal stress on the power semiconductors and is therefore the critical operating point that determines the thermal management and heatsink design of the system.

CHAPTER VI
IMPLEMENTATION OF DIGITAL CONTROL

The critical metrics of power electronics systems, such as performance, efficiency, and flexibility, depend largely on the control strategy applied. Traditional analog controllers, despite being simple and fast, have disadvantages such as sensitivity to environmental conditions (temperature, component aging, etc.), sensitivity to noise, and difficulties in applying complex control algorithms.

In aviation applications, it is almost mandatory for LRU (Line Replacement Unit) devices to include a decision-making unit (MCU or FPGA). Requirements such as multiple communication interfaces, debugging features, and reporting of detected errors to the external environment make the use of an MCU or FPGA mandatory. Additionally, the decreasing costs of controllers in recent years have increased the frequency of their use.

Digital control enables voltage and current regulation of the converter to be performed in a digital and more flexible environment by assigning an additional role to the controller currently used within the LRU.

6.1 OVERVIEW OF CONTROL STRATEGY

The control of an LLC resonant converter essentially aims to maintain the output voltage or current at a specific reference value. The most distinctive feature of an LLC converter is that its gain can be adjusted by changing the switching frequency. The general control strategy is based on a closed-loop feedback structure. The basic steps of this structure are as follows:

1. **Sensing:** The output voltage (Vout) and output current (Iout) of the charger are measured periodically using appropriate sensors and an analog-to-digital converter (ADC). The frequency of this period is one of the factors that will determine the response of the converter.
2. **Error Calculation:** The measured value is compared with the target reference value (Vref or Iref) to generate an error signal. Since the charging process of

lithium-ion batteries typically involves Constant Current (CC) and Constant Voltage (CV) modes, the controller must be capable of switching between these two modes.

3. **Controller**: The error signal is processed by one or more compensators. The main purpose of the controller is to produce an output that will reduce the error signal to zero.
4. **Modulator**: The controller's output is connected directly to a PFM block. This block converts the digitally calculated switching frequency into a square wave. The frequency of the square wave must be equal to the calculated digital frequency value.
5. **Driver:** The calculated frequency value is loaded into the hardware unit (usually a timer/PWM module) that generates the high-resolution PWM signals required to drive the FET switches on the primary side of the converter.

6.2 SELECTION OF DIGITAL CONTROLLER PLATFORM

The efficient, effective, and flexible implementation of a digital control strategy depends on selecting the right hardware platform. In particular, some MCU models are specifically designed for power electronics control. For example, Texas Instruments' C2000 series is one of the suitable series for this type of converter, featuring high-resolution and easily configurable PWM modules and fast ADC modules.

For the LLC charger developed in this thesis, a high-performance C2000 series TMS320F2837x series processor will be used. The following critical features were targeted in making this selection:

High Processing Power: High MIPS processing capacity for fast control loops and effective execution of the PI algorithm.

Floating Point Unit: FPU provides greater convenience and flexibility for software that works with numbers, eliminating the need for bit-wise processing when working with decimal numbers.

High-Resolution PWM: This PWM module, which offers nanosecond-level resolution for frequency modulation and deadband adjustment, will greatly simplify the creation of digital control software. Additionally, the use of multiple modules that can operate synchronously will enable synchronous rectification to be performed using a digital controller. Furthermore, protection methods such as "Trip Zone" will allow

us to easily and safely stop the converter's operation in the event of an unwanted situation.

ADC: The high-resolution and high-speed ADC module will improve both the regulation of the converter and its response time.

Different Communication Modules: Diversified communication modules will assist in designing both internal communication and external interfaces.

6.3 FREQUENCY MODULATION CONTROL ALGORITHM

The basic control mechanism of the LLC resonant converter is based on changing its gain by adjusting the switching frequency. The voltage gain of the converter is a complex function that depends on parameters such as normalized frequency (Fx), quality factor (Q), and inductance ratio (m). This gain expression is specified in Equation (5.7) This equation creates the gain curves that characterize the behavior of the LLC converter. The main goal of the control algorithm is to navigate these curves to achieve the desired output voltage.

6.3.1 PI Controller Design

A PI controller will be used in the feedback loop as a numerical controller. The ideal PI controller expression in the continuous time domain:

$$u(t) = Kp * e(t) + Ki\int e(t)dt \tag{6.1}$$

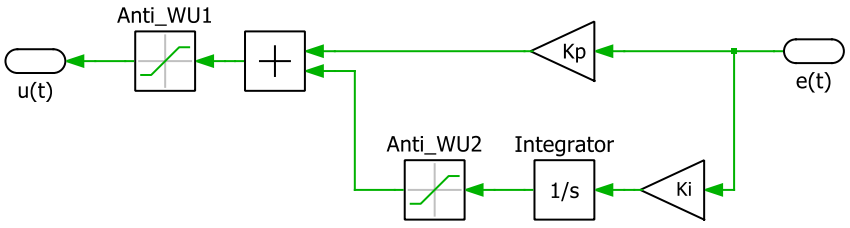

Figure 13: PI Controller Design

Here, Kp is the proportional gain, and Ki is the integral gain. On a numerical platform, the discrete-time domain counterpart of this equation is applied. Discretization can be performed using methods such as backward Euler or Tustin (bilinear) transformation. The commonly used discrete-time PI algorithm is as follows:

$$u[n] = u[n-1] + Kp(e[n] - e[n-1]) + KiTse[n] \tag{6.2}$$

Here:

- u[n]: Controller output at the nth sampling instant (frequency value or intermediate value determining the frequency).
- u[n−1]: Previous controller output.
- e[n]=Vref−Vout[n]: Error at the nth sampling instant.
- Ts: Sampling period (operating period of the control loop).
- Kp and Ki: The tuned gain coefficients of the digital PI controller.

Anti-Windup Mechanism: In PI controllers, especially when the system reaches saturation (e.g., when the maximum or minimum frequency limit is reached), the integral term accumulates uncontrollably ("windup"). This causes the system to respond slowly after reaching saturation. To prevent this, an anti-windup mechanism that stops or limits the accumulation of the integral term when the controller output reaches the limits must be integrated into the control loop.

6.4 CONTROL LOOP SYSTEM DESIGN

Basically, a power converter is a device that changes one type of electric power into another. Its main function is to maintain its output level, independent of any changes in the supply voltage or load. To be able to achieve this, a power converter needs a dynamically stable closed-loop control system. The digital closed-loop control loop for the LLC resonant converter will be the subject of this section.

If we look at the control loop as a system with inputs and outputs, the charger will need two inputs: output voltage and output current. The main task of this loop will be to control these inputs so as to operate the CC/CV charging function. To achieve this function, we will need to generate a variable frequency output from these two inputs. This is because LLC converters are a type of converter controlled by Pulse

Frequency Modulation, which generates an output voltage according to a variable frequency. As shown in Figure 14, the analog frequency output generated by the Control Loop can be converted into a digital signal by the Modulator and used as a control signal for the FETs.

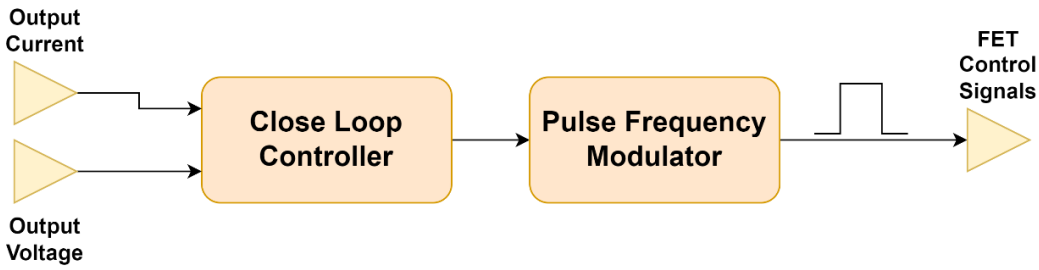

Figure 14: Closed-Loop Control System

6.4.1 Close Loop Controller

The Closed-Loop Controller incorporates all decision-making and calculation functions of the system. Its task is to process the output voltage and output current feedback signals from the power stage, compare this data with the target reference values, and generate the final frequency command to be sent to the PFM (Pulse Frequency Modulation) modulator by applying the logic required by the battery charging algorithm. The internal structure of the controller block, its functional units, and its operating principle will be clarified in detail in this part of the article.

To be able to make the correct decision, the controller needs to measure the controlled quantities accurately. This block performs the processing of two main feedback signals: output voltage (Vout) and output current (Iout).

Voltage Sensing: Output voltage is obtained by a high-impedance resistor divider circuit that is connected directly to the output. The main purpose of the circuit is to convert the high output voltage to the voltage level acceptable for the microcontroller ADC unit. Hence the system receives the output voltage information.

Current Sensing: Usually output current is found by measuring the voltage produced as the current passes a low-impedance resistor. The voltage across the resistor is first differential amplified and then converted to the range which the microcontroller ADC unit can read.

The Close Loop Controller consists of two serial compensators, as shown in Figure 15. The input of the Voltage Loop Compensator is called V_error. V_error represents the difference between VREF and VOUT. Voltage regulation is achieved by keeping this difference close to zero. The constant voltage mode in the battery charging profile is provided by the Voltage Loop Compensator. The output of the Voltage Loop Compensator is used as the input of the Current Loop Compensator. This input is also referred to as IREF, or current reference. The current reference is

provided by limiting the output of the Voltage Loop Compensator. Since the output cannot exceed this limit, IREF is set to the maximum value.

The difference between IREF and IOUT, i.e., the output current, gives us I_error. This difference is used as the input to the Current Loop Compensator. The compensator attempts to reduce this error to zero. It does this by generating a frequency output. The Current Loop Compensator ensures a constant current charging mode.

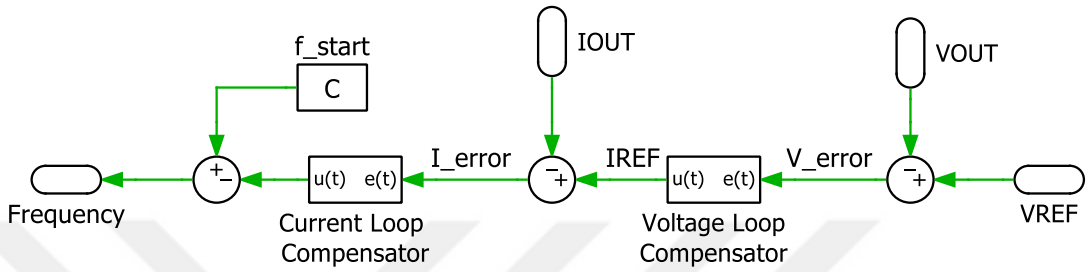

Figure 15: Voltage and Current Loop Compensator Design

6.4.2 Pulse Frequency Modulator

The final and most critical application layer of digital control architecture is the Pulse Frequency Modulator. This block acts as an "actuator" that takes a high-level, abstract digital command generated by the Closed-Loop Controller and converts it into low-level, precisely timed physical signals required to drive the semiconductor switches in the power stage. The modulator is also where the deadband is set. The figure shows a simulation of a PFM on PLECS. The duty is always entered as a fixed value of 50%. The frequency input receives the digital command generated by the closed-loop controller. This command is converted into two separate signals, PWM_HIGH and PWM_LOW. The deadband between these signals is set using the turn-on delay block in PLECS.

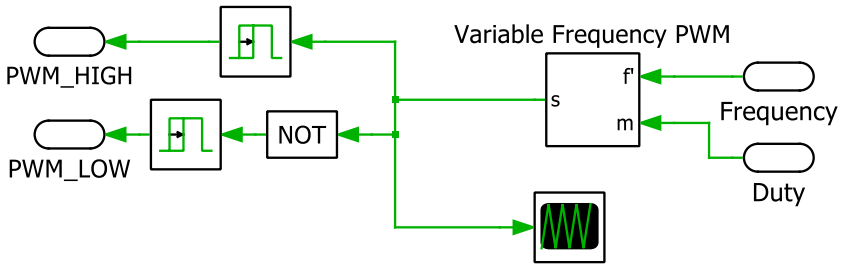

Figure 16: Pulse Frequency Modulator

PFM will be provided using the registers of the EPWM block within the selected processor [30]. The output of the control block will be converted into a period value. The frequency register of the EPWM will be continuously updated [30].

CHAPTER VII
SIMULATION OF LLC CHARGER

7.1 INTRODUCTION TO SIMULATION OF LLC CHARGER

The design and development process of power electronics systems consists of complementary stages such as theoretical analysis, simulation, and hardware prototyping. Simulation is the most important verification work among all these stages which is done before the theoretical design can be taken to the field. The complicated power electronics topologies as well as the digital control algorithms managing them can be conceived and verified with the help of advanced simulation tools. Thus, it becomes possible to detect the faults which are likely to happen during the design phase, to make an initial prediction of the system's dynamic behavior, and to change the controller parameters so that performance can be optimized.

Here performance metrics are considered that will be reflected through this section:

- **Steady-State Analysis:** This is the main instrument for checking the basic operating principles and converter waveforms under normal conditions.
- **Zero Voltage Switching (ZVS) Analysis:** Proving that ZVS, the main benefit of the LLC topology, is successfully accomplished in a broad region of load and input voltage variation.
- **Dynamic Performance Analysis:** The time and the stability of the system's reaction to the abrupt load and line voltage changes are being assessed.

These simulations works are a solid demonstration that the charger designed is capable of performance criteria targeted and thus, it is the required confidence to move further to the hardware prototype stage.

7.2 SETUP AND PARAMETERS OF THE SIMULATION MODEL

Precisely, the ability to reproduce the results of the performance evaluations in all cases is contingent upon the proper establishment of the simulation model that is at the base and the unambiguous delineation of the parameters of the system. This

subsection introduces the simulation environment used in the analyses, the structure of the model, and the numerical parameters that form the basis of the design. The model will be detailed enough to provide a foundation for validating LLC calculations and to give us a preview of the experimental results of the control algorithm.

7.2.1 Simulation Software and Model

The analyses were performed using the PLECS software package, which is renowned for its high accuracy and speed in the field of switched-mode power supply and control system simulation. PLECS provides an ideal environment for this study thanks to its ability to efficiently combine semiconductor models with ideal and thermal properties, magnetic components, and discrete-time control systems on the same schematic. The model established is a direct simulation counterpart of the power stage and digital controller blocks described in the previous sections.

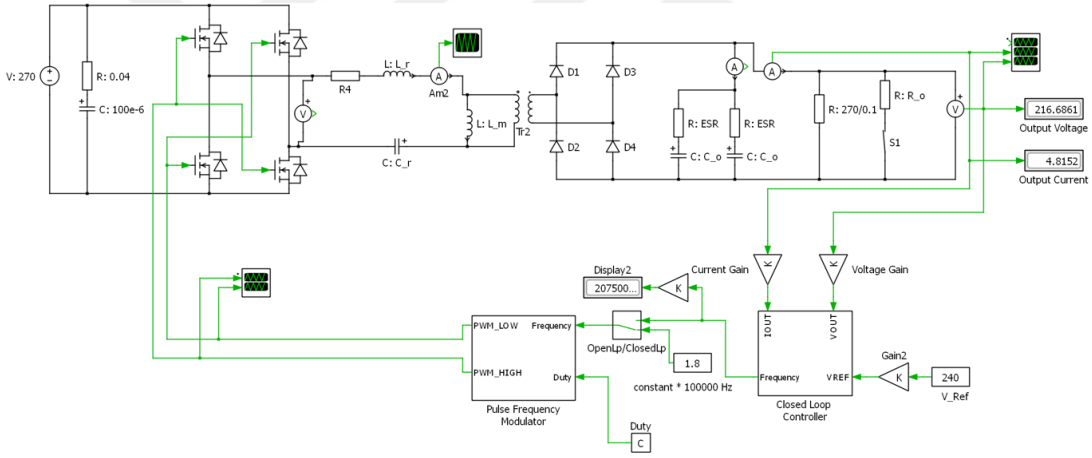

Figure 17: LLC Power and Control Stage Simulation Model

The model shown in Figure 17 above includes all electrical and control behaviors of the system. The power stage has been modeled to demonstrate the frequency responses of the product and to validate the selection of magnetic components. The digital controller block is a subsystem that incorporates the CC-CV logic, PI compensators, and PFM modulator designed in previous sections.

7.2.2 Basic Design and Simulation Parameters

The table below summarizes the key system parameters used in the simulations and calculated in the design section of the thesis. All analyses presented throughout this section are based on these reference values.

Table 4: Fundamental Design and Simulation Parameters

Parameters	Values	Description
Lm	110 uH	The magnetizing inductance of the transformer. This is the component that operates the parallel element in the resonant tank and is very important for attaining Zero Voltage Switching, especially when the load is light. The value of this component also determines the converter's gain curve.
Lr	22 uH	Inductance of the series resonant circuit. Together with the resonant capacitor, it forms the main series resonant tank. This element alone is basically the one to make the current waveform sinusoidal and to decide its maximal value.
Cr	72 nF	The main series resonant tank is formed by the series resonant capacitance along with the resonant inductor. The component allows the resonant action to proceed by storing and transferring energy during every cycle, thus enabling the sinusoidal current flow.
n	1	The main-to-secondary coil turns ratio of the transformer. It defines the standard voltage level change of the system and is the main factor in determining the load-dependent quality factor.
I_limit	6A	The target output current for the Constant Current charging mode. This value serves as the reference for the controller's current feedback loop.
V_limit	275V	This is the voltage level that the Constant Voltage charging system aims for. The single-cell battery voltage at this point is considered the fully charged state and the controller uses this voltage as the reference for its feedback loop.
fr	126.5 kHz	The natural resonant frequency of the series resonant tank. It constitutes the central point of the converter's gain curve. The switching frequency is modulated around this value to regulate the output. This frequency is determined by the series resonant inductor and capacitor values.

7.3 VERIFICATION OF POWER BLOCK DESIGN BY SIMULATION

7.3.1 Introduction to Verification

In this section, the aim is to verify the basic electrical characteristics of the designed LLC converter power block independently of the controller.

In order to systematically carry out this verification process, an open-loop test methodology will be adopted. In this methodology, the closed-loop controller will be disabled, and a signal generator with a manually adjustable frequency will be connected directly to the PWM inputs of the power stage. This approach allows us to analyze the natural response of the power stage in isolation, without the dynamic effects of the controller. In the simulation environment, this transition is achieved using a simple manual switch block, as shown in Figure 18.

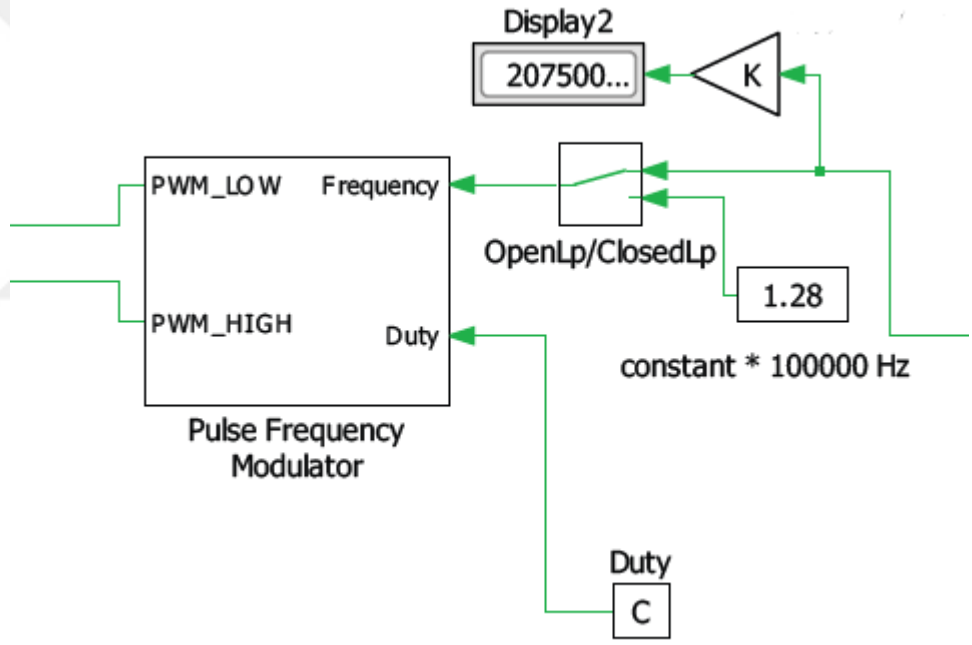

Figure 18: Open Loop Controller Block

7.3.2 Operating Analysis at Resonant Frequency (fs = fr)

The first step in power block verification is to confirm that the Lr and Cr components, which are elements of the resonance tank, are correctly designed. Theoretically, when an LLC converter is driven exactly at its resonance frequency (fs=fr), the input impedance of the resonance tank becomes purely resistive, and the voltage gain is approximately equal to the transformer conversion ratio.

To verify this theoretical expectation, while the system is operating at nominal input voltage and full load, the switching frequency is fixed at 126.5 kHz, which is the resonance frequency calculated in the design. Under these conditions, the following behaviors are expected:

1. The phase difference between the fundamental component of the square wave voltage applied to the tank input and the resonant current should be as small as possible. Theoretically, as the switching frequency approaches the resonance frequency, the tank impedance becomes largely resistive, and the phase difference minimizes. However, as a natural characteristic of the LLC topology, there is always a small phase shift between voltage and current due to the reactive current drawn by the magnetizing inductance.
2. The tank current should be as close to a perfect sine wave as possible.
3. The output voltage should be Vout≈Vin/n (n: transformer ratio).

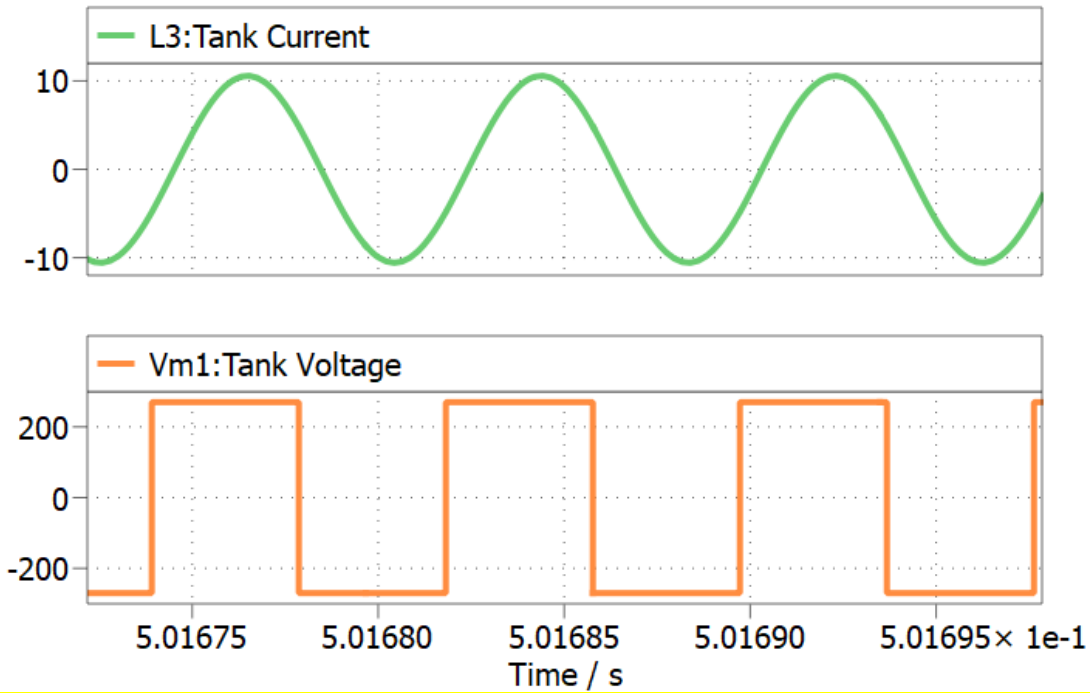

Figure 19: Resonant Tank Current and Voltage (fs = fr, Green: Tank Current, Orange: Tank Voltage)

Figure 19 examines operation at the resonant point (fs = fr). The first observation is that the resonant current, ILr, lags the applied square-wave excitation by a small phase angle. This is not a design defect; it is intrinsic to the LLC topology. The parallel magnetizing inductance, Lm, always draws a reactive magnetizing

current, so the tank impedance is not purely resistive even at exact resonance and the system exhibits a mildly inductive character.

The second and principal observation is the agreement with the expected voltage gain. The simulation reports Vout = 270 VDC. With Vin = 270 VDC and a unity transformer turns ratio, operation at fs = fr yields the anticipated gain K ≈ 1, which the result confirms.

Taken together, the theoretically explainable phase offset and the measured unity gain indicate that the resonant tank elements (Lr, Cr, Lm) and the transformer have been correctly designed, and that the simulation model faithfully captures the converter's real-world behavior.

7.3.3 Deriving the Voltage Gain Curve through Simulation

The previous section confirmed that the LLC converter matches theoretical behavior at a single operating point, the resonant frequency. For a PFM controlled architecture, overall performance depends on the gain varying in a predictable and stable manner across the entire switching frequency span. The digital regulation strategy is built on this frequency to gain relationship K as a function of fs, and robust output regulation requires that K change smoothly and monotonically within the range commanded by the controller.

To assess this, a simulation campaign is used both to validate the analytically derived gain curve and to verify compliance with the charger requirements. The goal is to verify that the measured gain follows the expected profile and remains within the limits that enable the controller to reach and maintain the target output voltage under nominal input conditions and a fixed load.

Validation follows a frequency sweep methodology. Using an open-loop testbench, the switching frequency fs is stepped across the intended operating band while the input voltage remains at its nominal value and the load remains constant. At each frequency point, transients are allowed to decay until steady state is reached, then the output voltage Vout is recorded. The experimental voltage gain for that point is computed from the recorded data, for example K equals Vout divided by n times Vin where n is the transformer turns ratio. The resulting data set yields an empirical curve K as a function of fs, which is compared directly with the theoretical prediction and used to check whether the converter, as configured, satisfies the charger operating requirements.

Table 5: Simulated LLC Converter Gain vs Frequency Ratio

Frequency (fs) [kHz]	Vout [V]	Calculated Gain (K)
90	338	1.252
100	310	1.148
110	290	1.074
120	277	1.026
126.5	270	1.000
130	265	0.981
140	254	0.941
150	243	0.900
160	234	0.867
170	224	0.829
180	216	0.800

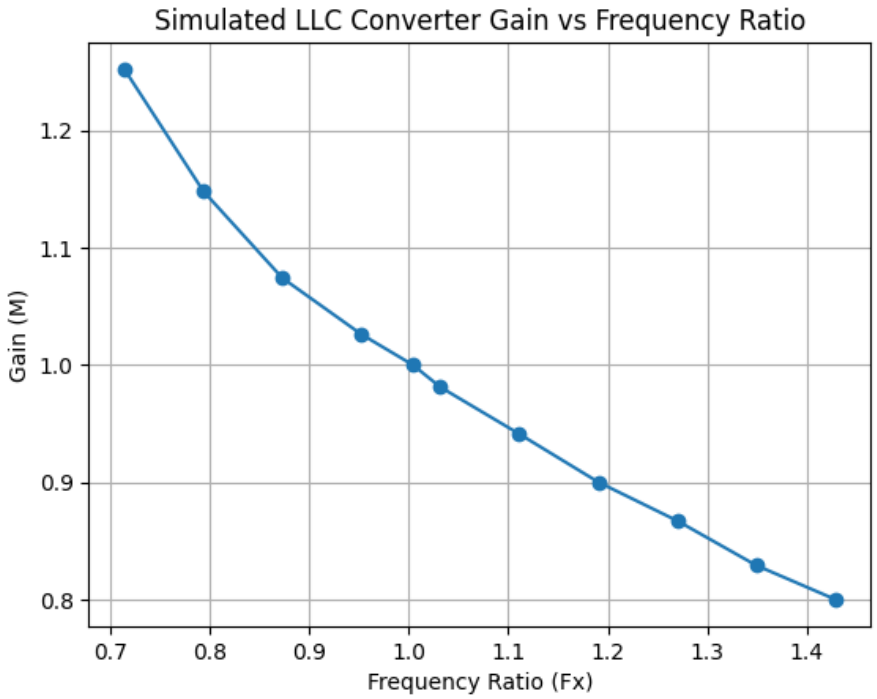

Figure 20: Simulated LLC Converter Gain vs Frequency Ratio

These results confirm the system's suitability for use as a charger. The battery described in Section 3.1.2 operates over 280 VDC to 230 VDC. The current design's frequency–gain characteristic comfortably covers this span and provides adequate margin for closed-loop regulation across the full input range.

Although the values appear suitable, several real-world factors can shift the frequency–gain characteristic, and many are difficult to capture in simulation.

1. Component tolerances: Manufacturing spreads in passive components cause deviations from nominal values. Tolerances of 10 to 15 percent can move the gain curve.
2. Current level: Inductors begin to saturate at higher currents. The effective inductance drops below its nominal value, which alters the gain curve.
3. Frequency dependence: Components exhibit different inductive and capacitive behavior at different frequencies. For example, an inductor impedance measured at 100 kHz will differ at 200 kHz, which changes the gain curve.

For these reasons, even when analytical and simulated results agree, it is prudent to design with margin. Tolerance-aware design reduces the likelihood of issues while meeting the target gain.

As analyzed previously, the gain at the resonant frequency of 126.5 kHz is again confirmed to be unity.

7.4 SIMULATION MODELING OF THE DIGITAL CONTROL SYSTEM

In the previous section, the fundamental electrical characteristics of the developed LLC converter power stage were verified in simulation using an open-loop test methodology, and the resonance and gain behaviors were analyzed and recorded. These analyses demonstrated that the plant behaves according to theoretical models and in a predictable manner, thereby providing a solid foundation for control design.

This section details how the digital control system described earlier was transferred to the simulation environment and modeled. The controller, whose theoretical basis and algorithmic structure were presented in previous sections, was implemented in PLECS and Simulink as functional blocks that represent the final firmware intended to run on a microcontroller or a digital signal processor.

The resulting digital control model includes all functional layers: from sensing and digitizing the feedback signals, through the dual-loop PI controller architecture that executes the constant-current and constant-voltage charging algorithm, to the PFM modulator that converts controller commands into physical drive signals.

7.4.1 General Structure of the Digital Controller

The simulation model of the digital controller was built using a modular approach. Each core function was implemented within its subsystem block, and these blocks were integrated to obtain the overall controller architecture shown in Figure 21.

This structure makes the relationships between software modules and the direction of data flow explicit and easy to trace.

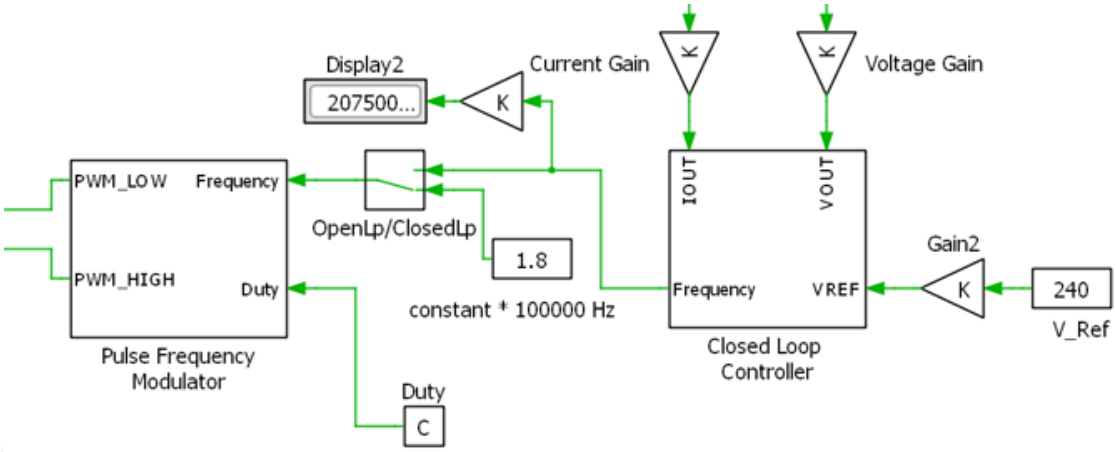

Figure 21: General Structure of the Digital Controller

As shown in Figure 21, the controller consists of three main functional blocks:

1. **Modeling of Feedback Signals:** A block that converts analog signals from the power stage into a form suitable for the digital processor.
2. **CC-CV Control Logic and PI Compensators:** The system's decision-making mechanism.
3. **Digital PFM Modulator:** A block that converts decisions into physical action.

7.5 SIMULATION ANALYSIS OF CLOSED-LOOP SYSTEM PERFORMANCE

7.5.1 Constant Current (CC) and Constant Voltage (CV) Mode Regulation Performance

The longest and most energy-transfer-intensive phase of a battery charge is the Constant Current mode, abbreviated CC. In this phase, the charger's primary task is to regulate a fixed output current independent of the instantaneous battery voltage. The ability of the closed-loop controller to perform this task stably has a direct impact on total charge time and long-term cell health.

This section evaluates the CC-mode regulation performance of the developed LLC charger under closed-loop control. The first objective is to test how accurately the output current tracks its reference under varying load conditions. In this operating

regime, the current control loop, implemented as a proportional–integral regulator, is expected to be dominant and to govern the overall system response.

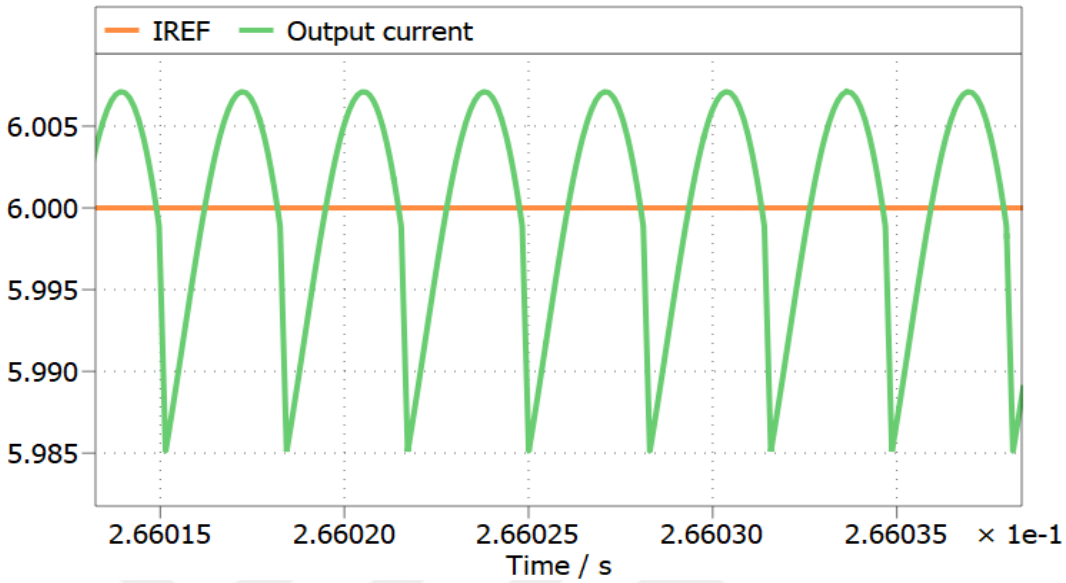

Figure 22: Constant Current (CC) Mode Regulation Performance

The waveform shows the output current while the system operates in steady-state CC mode. The charge current is limited to 6 A as the measured current follows the 6 A reference very closely. In the case of a low battery voltage, the controller increases the switching frequency in order to keep the same regulated current. With the charging advancing, the battery voltage gets higher; thus, to keep the current unchanged, the converter output has to go up. This rise is achieved by gradually lowering the switching frequency, which increases the stage gain.

Once the output voltage reaches its reference and the current starts to fall, the voltage PI loop becomes dominant. The controller holds the output at the set reference, establishing CV mode and ensuring a controlled transition from CC to CV.

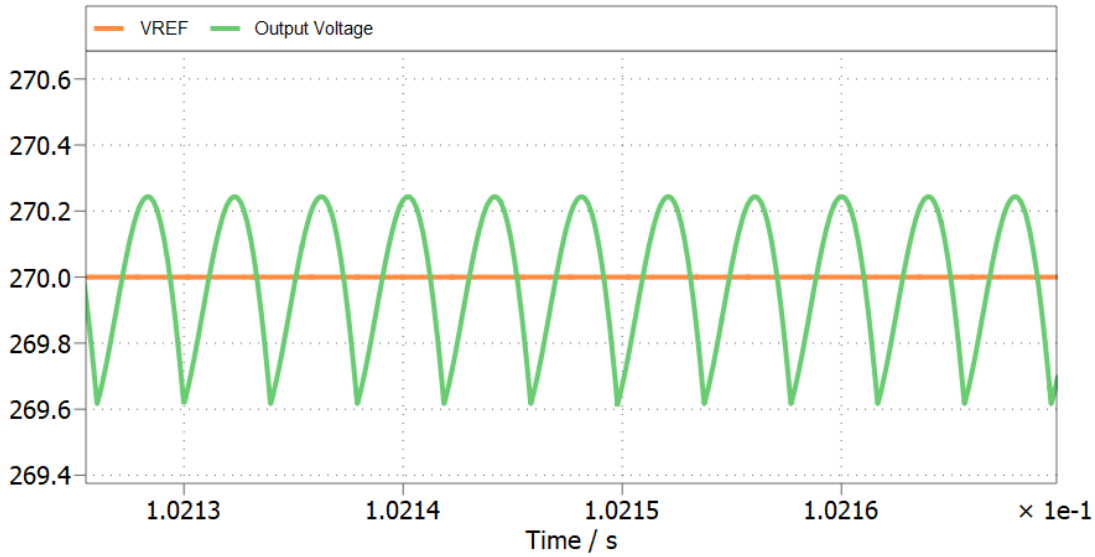

Figure 23: Constant Voltage (CV) Mode Regulation Performance

The waveform above shows the behavior of the output voltage while the system is operating stably in CV mode. As can be seen, the measured output voltage follows the constant voltage reference. In this case, the output current will gradually decrease. At some point, the charging process will end when the battery is fully charged.

CHAPTER VIII
EXPERIMENTAL RESULTS

In the previous chapters of this thesis, an LLC resonant converter-based power stage and a digital control system to manage this stage were designed for a battery charger powered by a 270V DC busbar, theoretical analyses were conducted and comprehensively validated in a simulation environment. The design and simulation phases provided strong predictions that the system met the targeted electrical and dynamic performance criteria.

This chapter presents the results of experimental tests on the hardware prototype, the final validation step of the design process. The primary objective of this chapter is to measure and characterize the performance of the manufactured physical prototype under real-world conditions and, most importantly, to prove the validity of the entire design and modeling process by comparing these experimental results with the simulation predictions obtained in the previous chapters.

Throughout this chapter, the test setup and prototype will be introduced, basic functional tests, steady-state operating waveforms, soft switching (ZVS) performance, CC-CV charging profile verification, and finally, the device's efficiency at different loads will be demonstrated with concrete data. These test results will demonstrate that the device and topology can be used as both an efficient converter and battery charger on aircraft 270VDC lines.

8.1 TEST SETUP AND PROTOTYPING

In this subsection, the laboratory environment where the tests were performed and the hardware prototype on which the measurements were made are introduced.

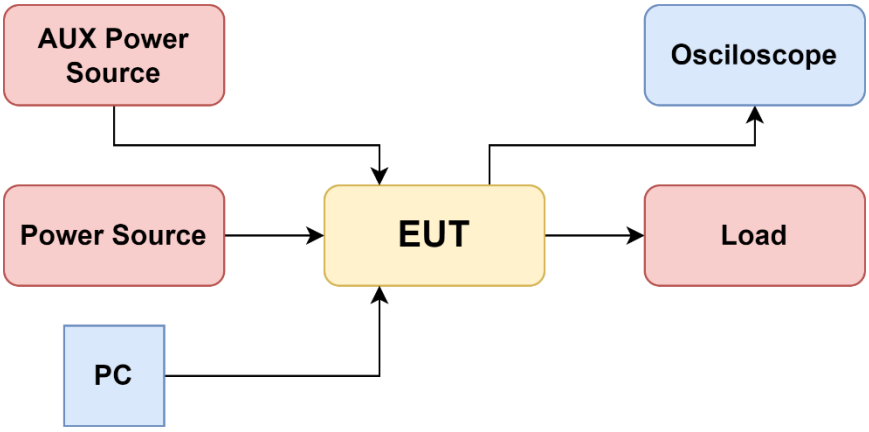

Figure 24: Test Setup

8.2 VERIFICATION OF CONTROL SIGNALS

Before testing the prototype under high power, the control signals were examined to ensure that the digital controller was correctly generating the basic PWM signals.

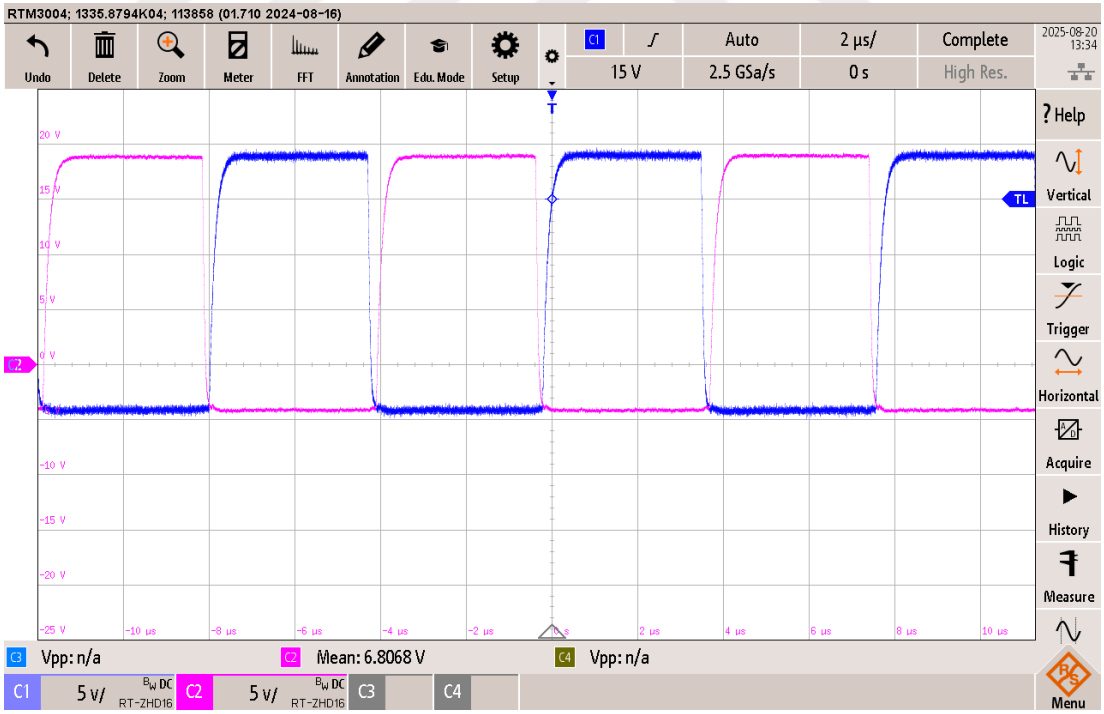

Figure 25: Primary-Side Gate Drive Signals (Vgs1, Vgs2) at 128 kHz, Scale: 2us

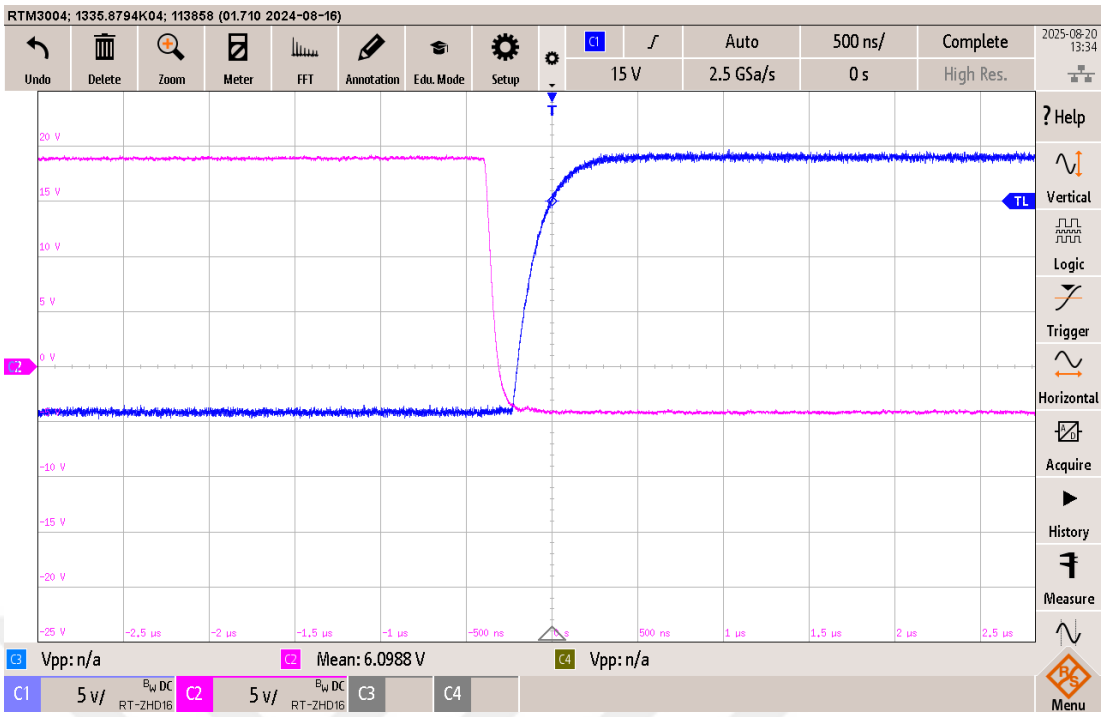

Figure 26: Primary-Side Gate Drive Signals Vgs1 Turn on Deadband at 128 kHz, Scale: 500ns

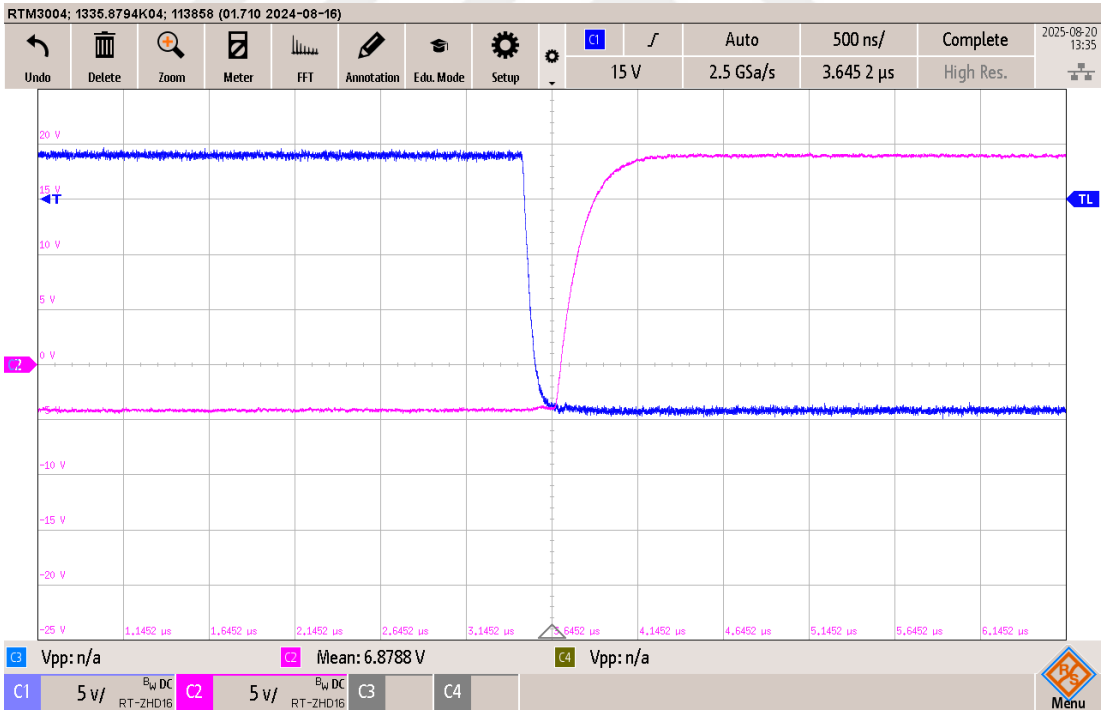

Figure 27: Primary-Side Gate Drive Signals Vgs2 Turn on Deadband at 128 kHz, Scale: 500ns

The figures above show two complementary signals for driving the primary-side full-bridge switches. Measurements were taken at resonant frequencies. The duty cycle of the signals was confirmed to be very close to 50%. Zooming in on the image

clearly reveals the dead time between the falling edge of one signal and the rising edge of the other.

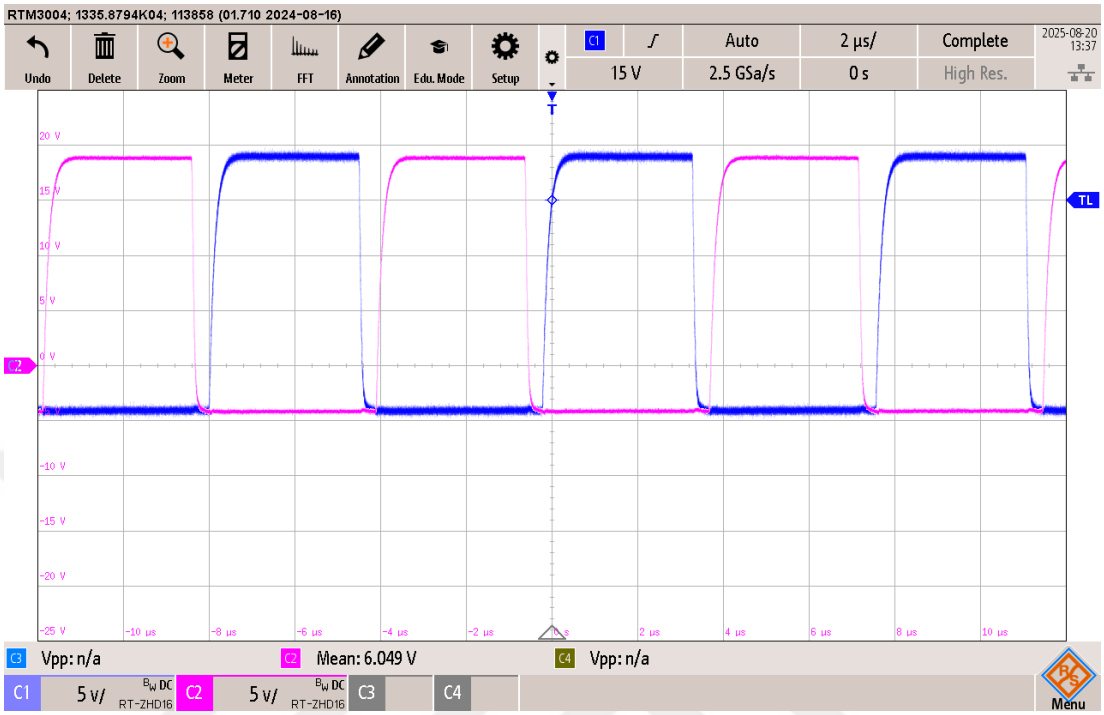

Figure 28: Primary-Side Gate Drive Signals (Vgs1, Vgs2) at 120 kHz, Scale: 2us

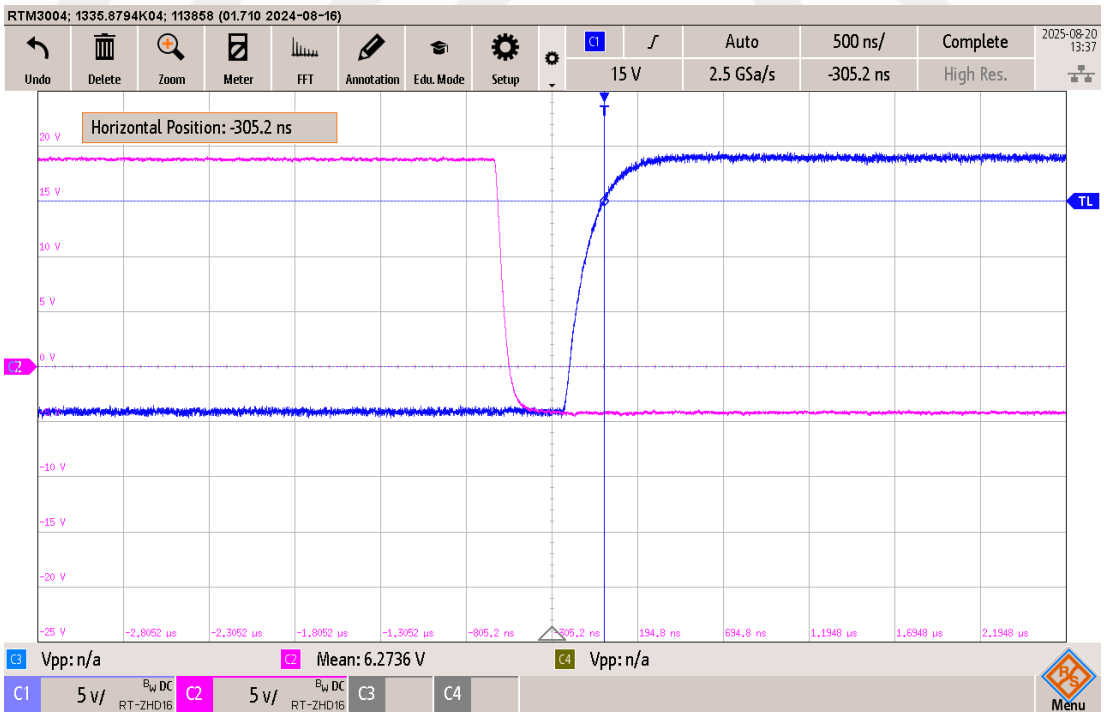

Figure 29: Primary-Side Gate Drive Signals Vgs1 Turn on Deadband at 120 kHz, Scale: 500ns

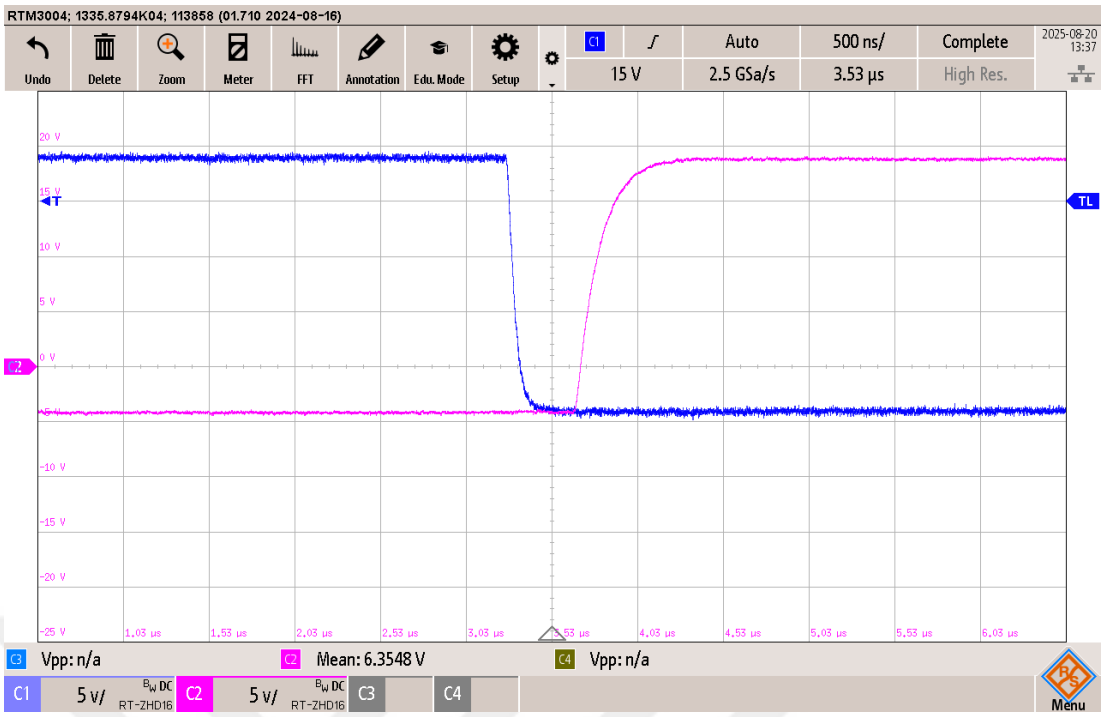

Figure 30: Primary-Side Gate Drive Signals Vgs2 Turn on Deadband at 120 kHz, Scale: 500ns

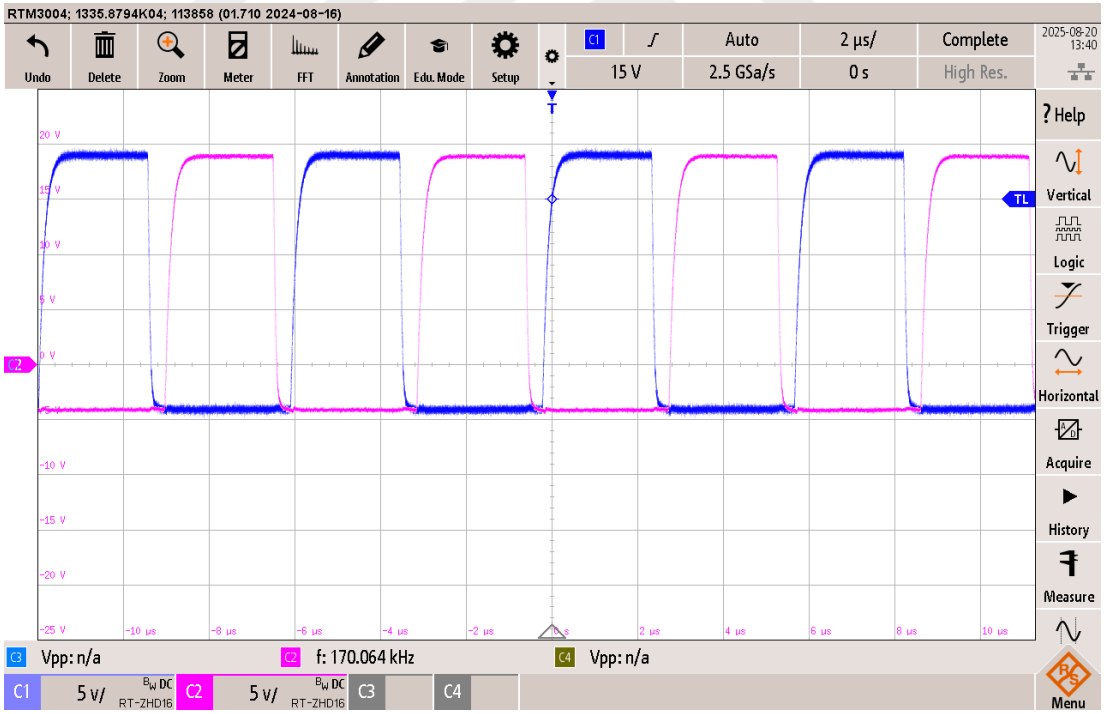

Figure 31: Primary-Side Gate Drive Signals (Vgs1, Vgs2) at 170 kHz, Scale: 2us

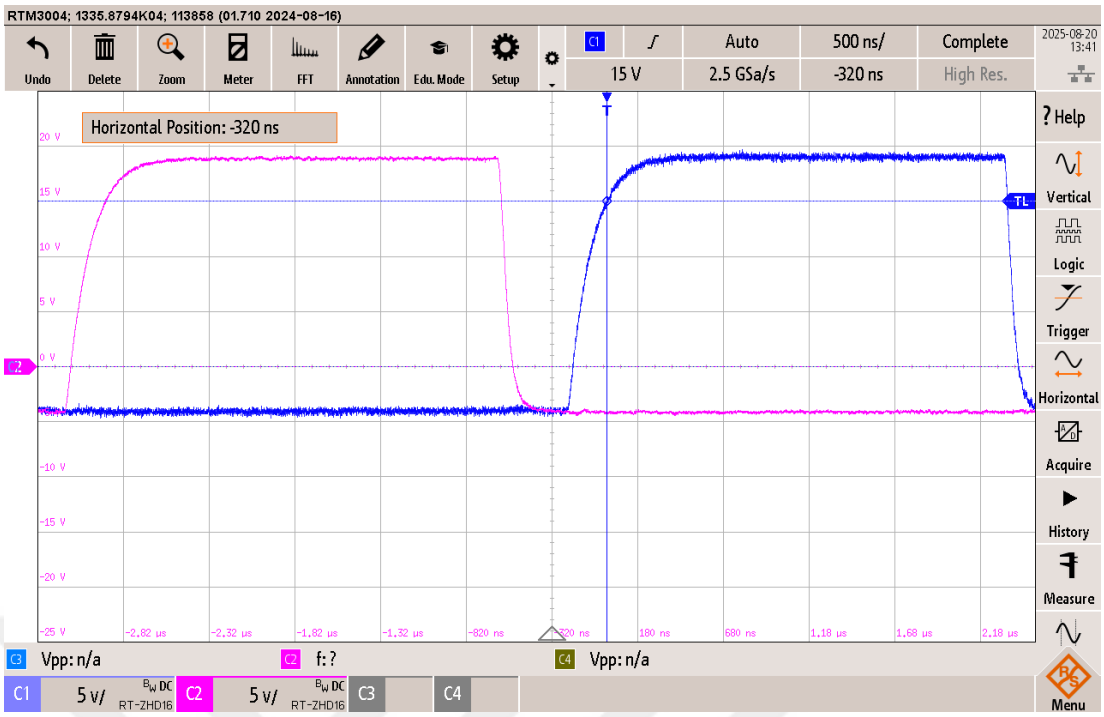

Figure 32: Primary-Side Gate Drive Signals Vgs1 Turn on Deadband at 170 kHz, Scale: 500ns

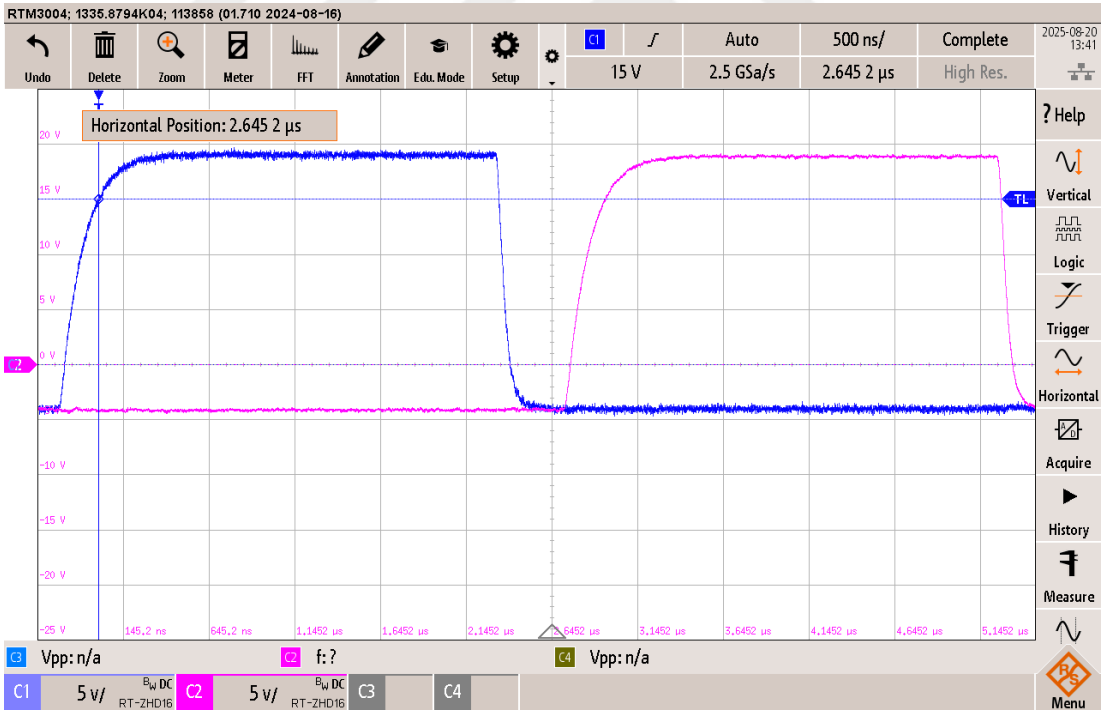

Figure 33: Primary-Side Gate Drive Signals Vgs2 Turn on Deadband at 170 kHz, Scale: 500ns

Measurements were made at the maximum and minimum frequencies to be tested in the figures above, and no problems were observed with the FET control signals on the primary side for the continuation of the tests.

8.3 STEADY STATE WAVEFORMS

This section presents the basic electrical waveforms generated by the converter during steady-state operation at nominal input voltage and full load. Waveforms taken at different operating frequencies will both test the system and verify its behavior at different charging voltages.

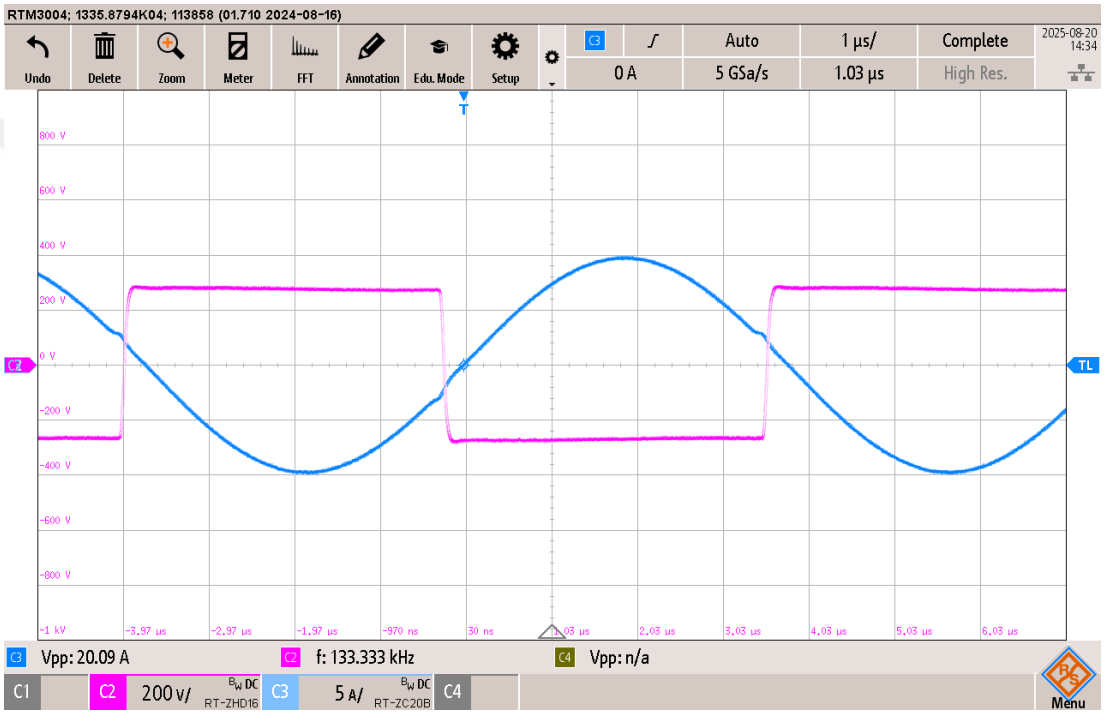

Figure 34: Resonant tank Voltage and Current at Resonant Frequency

In Figure 34, blue is the tank current, and pink is the tank voltage. This measurement, taken at a frequency very close to the resonant frequency, shows a sinusoidal tank current synchronous with the tank voltage.

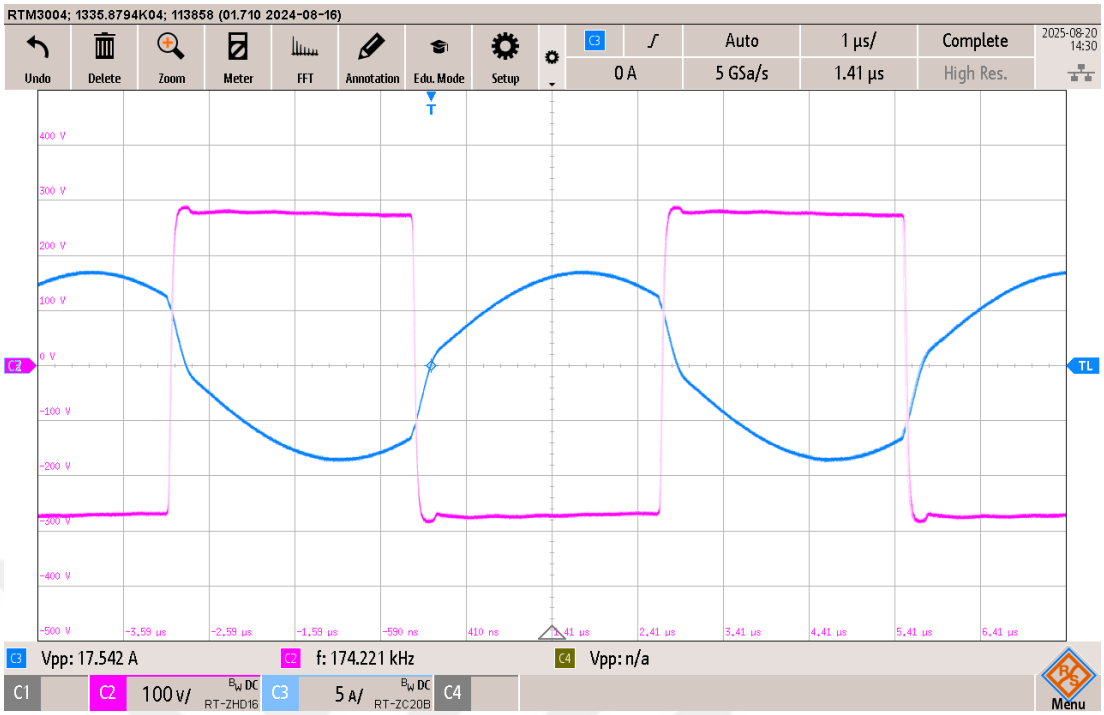

Figure 35: Resonant tank Voltage and Current above Resonant Frequency

In Figure 35, blue represents tank current and pink represents tank voltage. This measurement, taken at the charger's planned maximum operating frequency, shows the tank voltage and the deteriorating tank current. This current, above the resonant frequency, indicates that the charger is operating in step-down mode.

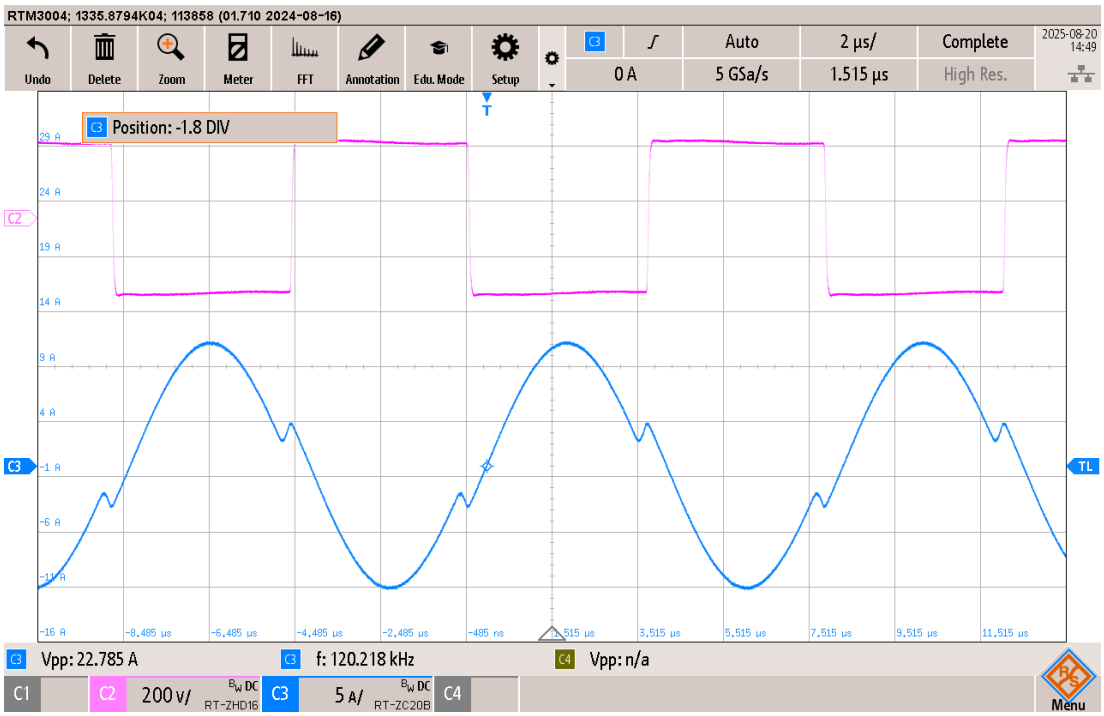

Figure 36: Resonant tank Voltage and Current below Resonant Frequency

In Figure 36, blue is the tank current, and pink is the tank voltage. This measurement, taken at the minimum frequency at which the charger is planned to operate, shows the tank voltage and the deteriorating tank current. This current, below the resonant frequency, indicates that the charger is operating in step-up mode.

8.4 SOFT-SWITCHING PERFORMANCE

Verifying ZVS performance in hardware, one of the most critical design objectives, is the focus of this section. In this section, we will demonstrate ZVS performance by measuring the Vds voltage and Vgs voltage on the system's primary switch at different operating frequencies.

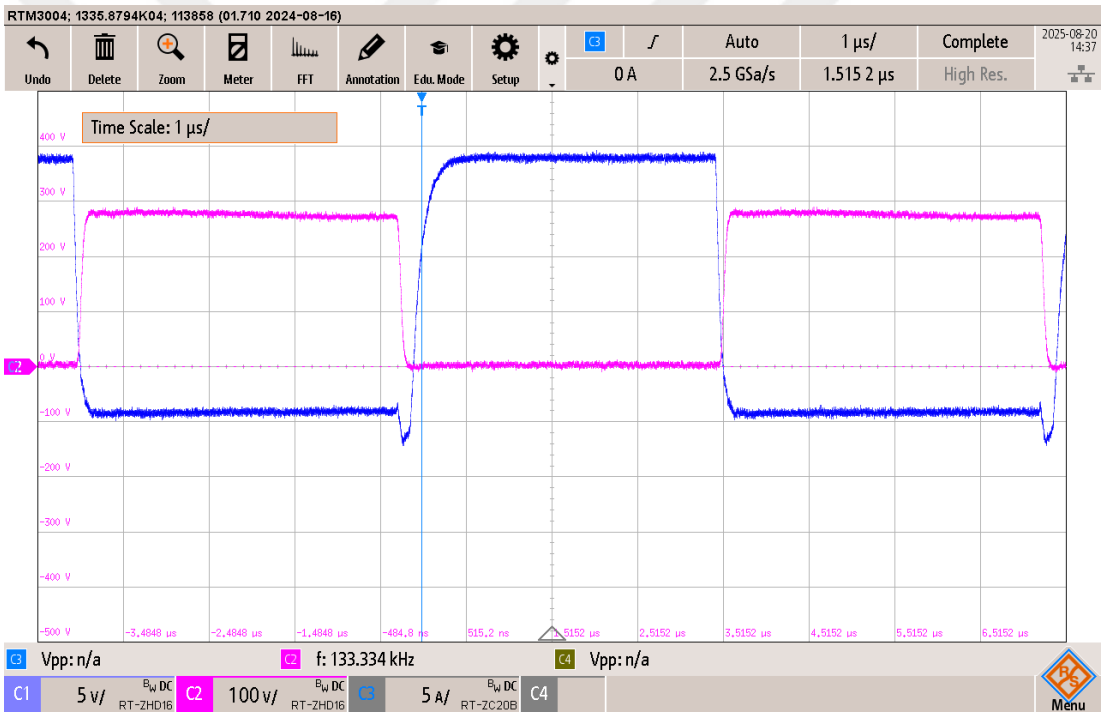

Figure 37: Primary-Side FET Vgs and Vds Signals at 133 kHz

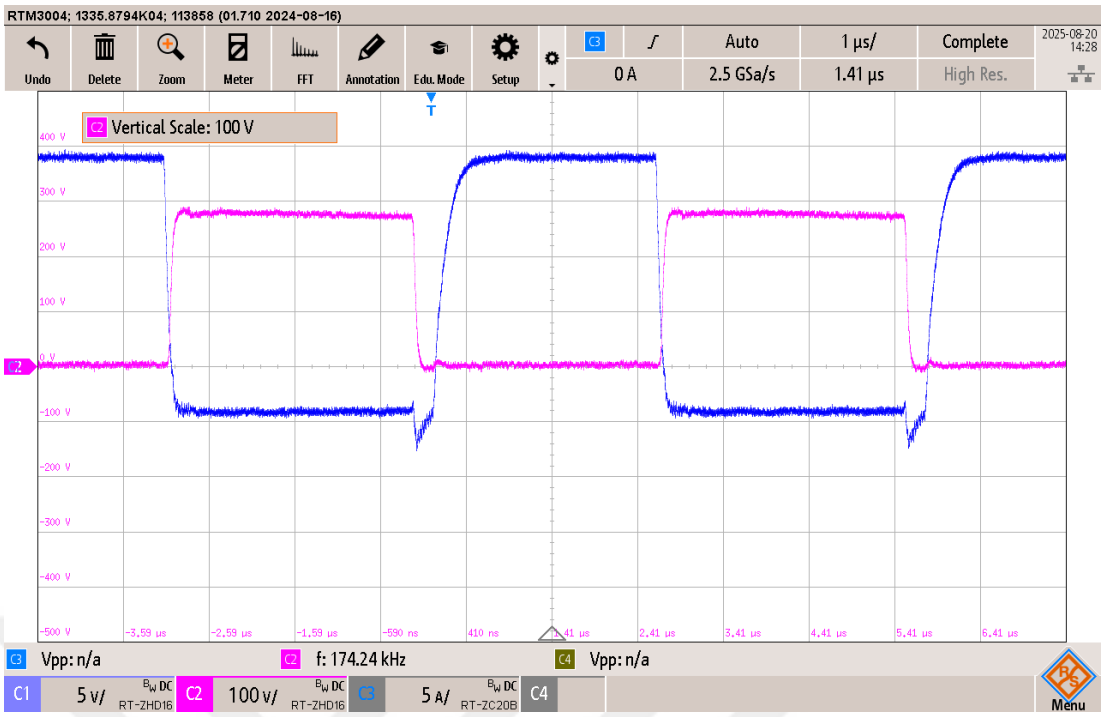

Figure 38: Primary-Side FET Vgs and Vds Signals at 174 kHz

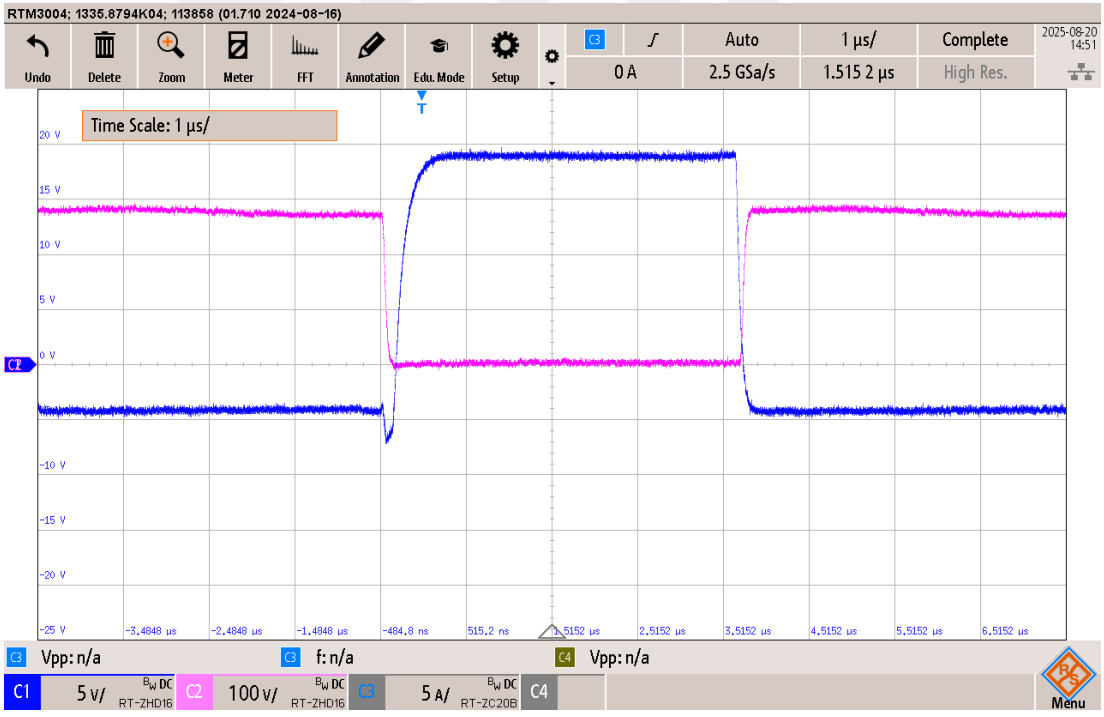

Figure 39: Primary-Side FET Vgs and Vds Signals at 120 kHz

As seen in Figures 37, 38, and 39, when the gate signal Vgs begins to rise to trigger FET conduction across the entire operating frequency range, it is clearly seen that the drain-to-source voltage Vds has already fallen to zero volts. This definitively demonstrates the successful implementation of Zero Voltage Switching (ZVS),

meaning the switch conducts with no voltage present, virtually eliminating turn-on switching losses.

8.5 CHARGE PROFILE (CC/CV) VERIFICATION

This section tests the charger's primary function its ability to successfully complete a full charge cycle. Tests were conducted using a discharged battery pack or a battery simulator capable of simulating this profile.

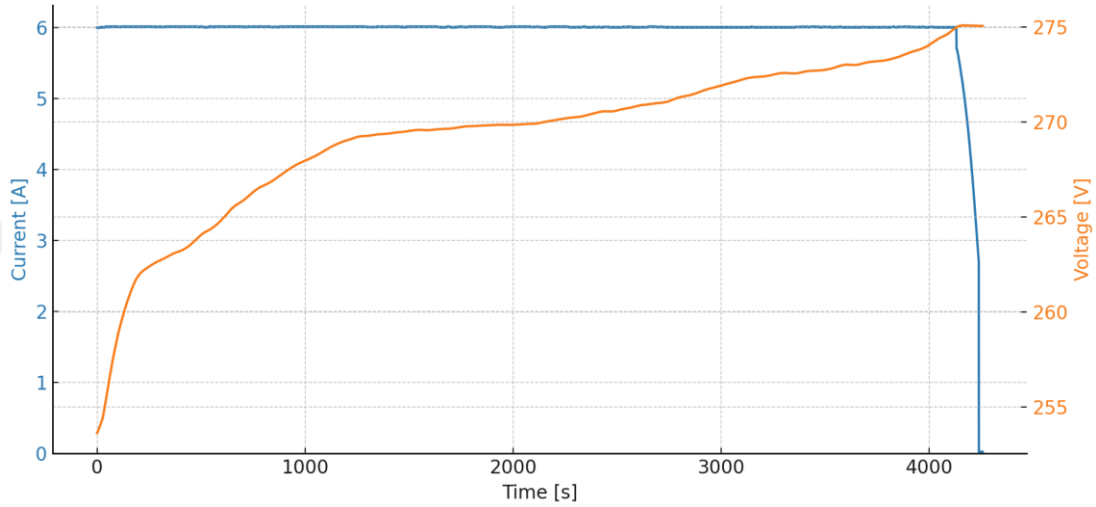

Figure 40: Voltage and Current Profile During CC–CV Charging

The graph shown in the figure is the CC/CV graph of a completely discharged 7.5 Ah battery under a 6A limit charge. After 4250 seconds of charging, the battery was properly charged. Towards the end of the graph, it appears to switch to CV mode. It's also clear that the voltage is regulated at 275VDC in CV mode.

8.6 EFFICIENCY ANALYSIS

During battery charging, input and output powers were recorded at three different frequencies and the efficiency of the charger was calculated.

Table 6: Efficiency Results

Frequency (kHz)	Power Input (W)	Power Output (W)	Efficiency
128	1665	1622	%97.4
170	1563	1507	%96.4
120	1727	1677	%97.1

The table shows that the charger has the highest efficiency at the resonant frequency. Although we do not lose ZVS, the efficiency at different operating frequencies does not go below 96%.

CHAPTER IX
CONCULUSION

The key factor for a successful aerospace application is the least-sized, least-weight on-board equipment which can, in fact, be directly the performance of an aircraft. The electrification trend to aviation translated by a strong call for the design of the power electronic converters to be characterized by a high power density, and more compact structure with less cooling requirements. Thus, this dissertation is mainly a consequence of the spreading of lithium-ion battery technologies in an environment of the aircraft. An efficient and performing charger is the first building block of novel energy storage concepts for airborne applications. The work was focused on the design, simulation, and realization of an LLC resonant converter-driven charger for avionics. Among the many reasons recognized for LLC topology, the work primarily cites these three: soft-switching operation, high efficiency within a wide load range, as well as the ability to implement CC/CV lithium-ion battery charging profiles. This investigation attempted to cover systematically the design stages from resonant tank parameters selection and transformer design with planar magnetic structures to semiconductor technologies choices and control strategies implementation for aerospace requirements. At first, the proposed design was substantiated with computer simulations and then it was executed and tested in the laboratory.

The device under test presents excellent efficiency levels, up to 97%, thereby confirming the performance potential of LLC converters in the context of aerospace systems. The conduction and switching losses are quite significantly lowered by the high efficiency; however, what is more substantial is that the thermal management burden is directly alleviated. Consequently, one can find a significant shrinking of the cooling surface areas in terms of both size and weight which, in turn, brings about a very valuable contribution to the aircraft platforms where every gram of weight or cubic centimeter saved has its merit. The introducing planar transformer technology has enabled further space-saving without compromising the electrical isolation & electromagnetic compatibility requirements achievement.

The most significant outcome out of this work, however, is associating LLC topologies with the concepts of More-Electric Aircraft and Fully Electric Aircraft. In the survey of the literature sector, the aviation is characterized by a trend that is leaning more and more toward architectures of this kind where the power electronics will be the core of the Energy Distribution, Propulsion, and Actuation. In these conditions, the presence of effective and fault-tolerant chargers is absolutely crucial. The current dissertation provides further evidence supporting the point that not only LLC resonant converters can be employed for battery charging systems, but they can be in a way that brings maximum benefits to the aviation sector.

Besides this, the present research provides a model design method that is adaptable to various voltage and power levels and that can be changed according to the needs of the aircraft. The ability demonstrated here to smooth switch over a broad range of operation combined with high efficiency and low thermal stress, guarantees that the envisioned charger can be scaled and introduced into forthcoming aerospace platforms.

Summing up, this dissertation has been able to demonstrate an LLC-based aviation battery charging system to be a powerful, cost-effective, and space-saving candidate, and therefore it is in line with the electrification goals of aerospace. Consequently, by conducting a high-efficiency profile, which indirectly leads to the ease of the thermal management task, the proposed design can be instrumental in enhancing the onboard power systems' reliability and integration feasibility. The next step in the development of this study could be a drift toward fault-tolerant configurations coupled with advanced digital control schemes to optimize the performance under flight conditions.

REFERENCES

[1] BUTICCHI G., WHEELER P., and BOROYEVICH D. (2023), "The More-Electric Aircraft and beyond", *Proceedings of the IEEE*, Vol. 111, No. 4, pp. 356–370, DOI: 10.1109/JPROC.2022.3152995.

[2] TA L. A. D., DAO N. D., and LEE D. C. (2020), "High-Efficiency Hybrid LLC Resonant Converter for On-Board Chargers of Plug-In Electric Vehicles", *IEEE Trans. Power Electron.*, Vol. 35, No. 8, pp. 8324–8334, DOI: 10.1109/TPEL.2020.2968084.

[3] SHAFIEI N., ORDONEZ M., CRACIUN M., BOTTING C., and EDINGTON M. (2016), "Burst Mode Elimination in High-Power LLC Resonant Battery Charger for Electric Vehicles", *IEEE Trans. Power Electron.*, Vol. 31, No. 2, pp. 1173–1188, DOI: 10.1109/TPEL.2015.2420573.

[4] BHATTACHARYA S., WILLICH C., HOENICKE P., and KALLO J. (2021), "A Novel Re-configurable LLC Converter for Electric Aircraft", *In, Proceedings of the 2021 IEEE 12th Energy Conversion Congress & Exposition – Asia (ECCE-Asia 2021)*, IEEE, Singapore, pp. 32–37, Singapore. DOI: 10.1109/ECCE-Asia49820.2021.9479165.

[5] CHEN G., CHEN L., DENG Y., WANG K., and QING X. (2019), "Topology-Reconfigurable Fault-Tolerant LLC Converter with High Reliability and Low Cost for More Electric Aircraft", *IEEE Trans. Power Electron.*, Vol. 34, No. 3, pp. 2479–2493, DOI: 10.1109/TPEL.2018.2848297.

[6] CHEN W., RONG P., and LU Z. (2010), "Snubberless Bidirectional DC-DC Converter with New CLLC Resonant Tank Featuring Minimized Switching Loss", *IEEE Trans. Ind. Electron.*, Vol. 57, No. 9, pp. 3075–3086, DOI: 10.1109/TIE.2009.2037099.

[7] FAROOQ H., KHALID H. A., KHALID M. U., FAROOQI M. M., and MALIK Q. (2021), “Loss Analysis of Full Bridge LLC Resonant Converter with Wide Input Range Using Si and SiC Switches”, In: *Proceedings of the 2021 16th International Conference on Emerging Technologies (ICET 2021)*, IEEE, Islamabad, Pakistan, pp. 1–6, DOI: 10.1109/ICET54505.2021.9689841.

[8] SIMMERS B., GERADA C., RAJASHEKARA K., LASKARIDIS P., and SEKI N. (2023), “Special issue on all-electric and hybrid-electric flight”, *IET Electrical Systems in Transportation*, Vol. 13, No. 1, e12071, DOI: 10.1049/els2.12071.

[9] MOIR I. and SEABRIDGE A. (2008), *Aircraft Systems: Mechanical, Electrical and Avionics Subsystems Integration*, 3rd ed., Wiley, Chichester, U.K.

[10] LI K., EVANS P., and JOHNSON M. (2016), “SiC and GaN Power Transistors Switching Energy Evaluation in Hard and Soft Switching Conditions”, *In, Proceedings of the 2016 IEEE 4th Workshop on Wide Bandgap Power Devices and Applications (WiPDA)*, IEEE, Fayetteville, AR, USA, pp. 123–128, DOI: 10.1109/WiPDA.2016.7799922.

[11] PATTANAYAK T. and MAVRIS D. N. (2025), “Battery Technology in Aviation: Current State and Future Prospects”, *engRxiv preprint*, DOI: 10.31224/4220.

[12] DAMIANO A., PORRU M., SALIMBENI A., SERPI A., CASTIGLIA V., DI TOMMASO A. O., MICELI R., and SCHETTINO G. (2018), “Batteries for Aerospace: a Brief Review”, *Proc. AEIT 2018 International Annual Conference*, pp. 1–6, Bari, Italy. DOI: 10.23919/AEIT.2018.8577355.

[13] BARZKAR A. and GHASSEMI M. (2020), “Electric Power Systems in More and All Electric Aircraft: A Review”, *In, Proceedings of the 2018 AEIT International Annual Conference (AEIT 2018)*, IEEE, Bari, Italy, pp. 1–6, DOI: 10.1109/ACCESS.2020.3024168.

[14] FENG X., REN D., HE X., and OUYANG M. (2020), “Mitigating Thermal Runaway of Lithium-Ion Batteries”, *Joule*, Vol. 4, No. 4, pp. 743–770, DOI: 10.1016/j.joule.2020.02.010.

[15] MOHAMMED M. S., SALEH A. H., AL-QAYSI H. K., and VURAL R. A. (2024), “Finite Automated System to Design a High Efficiency LLC Resonant Converter System for 3 kW PV Solar Array”, *e-Prime – Advances in Electrical Engineering, Electronics and Energy*, Vol. 10, Art. no. 100770, DOI: 10.1016/j.prime.2024.100770.

[16] WEI Y., LUO Q., and MANTOOTH A. (2020), “Overview of Modulation Strategies for LLC Resonant Converter”, *IEEE Trans. Power Electron.*, Vol. 35, No. 10, pp. 10423–10443, DOI: 10.1109/TPEL.2020.2975392.

[17] YANG B., LEE F. C., ZHANG A. J., and HUANG G. (2002), “LLC Resonant Converter for Front End DC/DC Conversion”, *In, Proceedings of the 2002 IEEE Applied Power Electronics Conference and Exposition (APEC 2002)*, IEEE, Dallas, TX, USA, pp. 1108–1112, DOI: 10.1109/APEC.2002.989382.

[18] LU B., LIU W., LIANG Y., LEE F. C., and VAN WYK J. D. (2006), “Optimal Design Methodology for LLC Resonant Converter”, *In, Proceedings of the 2006 IEEE Applied Power Electronics Conference and Exposition (APEC 2006)*, IEEE, Dallas, TX, USA, pp. 533–538, DOI: 10.1109/APEC.2006.1620590.

[19] REZAII E. Y. and CARVALHO A. (2024), “Analytic Discrete State-Space Model of LLC Resonant Converter”, *e-Prime – Advances in Electrical Engineering, Electronics and Energy*, Vol. 9, Art. no. 100625, DOI: 10.1016/j.prime.2024.100625.

[20] STEIGERWALD R. L. (1988), “A Comparison of Half-Bridge Resonant Converter Topologies”, *IEEE Trans. Power Electron.*, Vol. 3, No. 2, pp. 174–182, DOI: 10.1109/63.4347.

[21] OUTEIRO M. T. and BUJA G. (2015), “Comparison of Resonant Power Converters with Two, Three, and Four Energy Storage Elements”, *In, Proceedings of the 2015 IEEE 41st Annual Conference of the Industrial Electronics Society (IECON 2015)*, IEEE, Yokohama, Japan, pp. 1406–1411, DOI: 10.1109/IECON.2015.7392297.

[22] VU V. B., TRAN D. H., and CHOI W. (2018), “Implementation of the Constant Current and Constant Voltage Charge of Inductive Power Transfer Systems with the Double-Sided LCC Compensation Topology for Electric Vehicle Battery Charge Applications”, *IEEE Trans. Power Electron.*, Vol. 33, No. 9, pp. 7398–7410, DOI: 10.1109/TPEL.2017.2766605.

[23] ABDEL-RAHMAN S. (2012), *Resonant LLC Converter: Operation and Design - Application Note AN 2012-09, V1.0*, Infineon Technologies, North America, Durham, https://www.infineon.com/assets/row/public/documents/24/42/infineon-design-example-resonant-llc-converter-operation-and-design-applicationnotes-en.pdf, DoA: 15.10.2025.

[24] SHEN Y., ZHAO W., CHEN Z., and CAI C. (2018), “Full-Bridge LLC Resonant Converter with Series-Parallel Connected Transformers for Electric Vehicle On-Board Charger”, *IEEE Access*, Vol. 6, pp. 13490–13500, DOI: 10.1109/ACCESS.2018.2811760.

[25] WANG H., DUSMEZ S., and KHALIGH A. (2014), “Design and Analysis of a Full-Bridge LLC-Based PEV Charger Optimized for Wide Battery Voltage Range”, *IEEE Trans. Veh. Technol.*, Vol. 63, No. 4, pp. 1603–1613, DOI: 10.1109/TVT.2013.2288772.

[26] DING H. (2025), *Design of Resonant Half-Bridge Converter Using IRS2795(1,2) Control IC, Application Note AN-1160,* International Rectifier, https://www.infineon.com/dgdl/an-1160.pdf?fileId=5546d462533600a40153559a85df1115, DoA: 15.10.2025.

[27] YANG X., XIAO L., WU Q., ZHAO W., and CHEN W. (2024), “An LLC-DAB Hybrid Converter With High Input-Output Voltage Ratio Based on an Integrated Matrix Transformer”, *In, Proceedings of the 2024 IEEE International Conference on Electrical Systems for Aircraft, Railway, Ship Propulsion and Road Vehicles & International Transportation Electrification Conference (ESARS-ITEC 2024),* IEEE, Naples, Italy, pp. 823–827**,** DOI: 10.1109/ESARS-ITEC60450.2024.10819754.

[28] TALESARA B., JAYAPAL R., SUSHEEL B., RAO S. N., and SINGH B. K. (2015), “Efficiency Enhancement of Flyback Converter Using Synchronous Rectification”, *In, Proceedings of the 2015 Annual IEEE India Conference (INDICON 2015),* pp. 1–5, IEEE, New Delhi, India, DOI: 10.1109/INDICON.2015.7443380.

[29] HONG L., MA H., WANG J., DU J., and WANG B. (2016), “An Efficient Algorithm Strategy for Synchronous Rectification Used in LLC Resonant Converters”, *In, Proceedings of the 2016 IEEE 42nd Annual Conference of the Industrial Electronics Society (IECON 2016),* pp. 2452–2456, IEEE, Florence, Italy, DOI: 10.1109/IECON.2016.7794135.

[30] TEXAS INSTRUMENTS (2024), *TMS320F2837xS Real-Time Microcontrollers*, Datasheet SPRS881K, https://www.ti.com/lit/ds/symlink/tms320f28377s.pdf, DoA: 10.08.2025.